# PURGE AND SECONDARY FLOW INTERACTION CONTROL BY MEANS OF PLATFORM CIRCUMFERENTIAL CONTOURING

by

MELISSA HARRIS
B.S. University of Central Florida, 2009

A thesis submitted in partial fulfillment of the requirements
for the degree of Master of Science in Mechanical Engineering
in the Department of Materials, Mechanical and Aerospace Engineering
in the College of Engineering and Computer Sciences
at the University of Central Florida
Orlando, Florida

Fall Term
2011

# ABSTRACT

This study presents an attempt to reduce the losses produced by the purge flow in a turbine stage by incorporating circumferential platform contouring. Two contours are proposed and compared against a baseline at different levels of swirl. The computational simulations were performed using a RANS three-dimensional Computational Fluid Dynamics code with the Shear Stress Transport turbulence model. The results of steady simulations demonstrate that for the first contour, when the flow is swirled to 50% of the rim speed, the purge flow exits the cavity with less cross flow. This in turn reduces the strength of the passage vortex. However, at swirl extremes of 0% and 100% the baseline has the best performance. The results show that a carefully designed platform has the potential to reduce losses when the operating condition is in the proximity of 50% swirl.

I would like to dedicate this thesis to my loving father Jose Joaquin Seco
for always encouraging me to excel beyond all expectations.

It is not through expectations that one succeeds but by following a dream.

To my God and Savior Jesus Christ who made me go through this, and held me up the entire way.

# ACKNOWLEDGMENTS

The author would like to thank Dr. Jay Kapat and Mr. Paul Spedaler for their continuous support throughout the development of this thesis. Thanks for your advice and for remaining faithful in critical moments. Special thanks also to Dr. Matthew Montgomery for sharing his valuable input and knowledge. Thankfulness and appreciation is also extended to Dr. Todd Ebert for his patience in teaching me how to "do" CFD.

Additionally, the author would like to thank her parents for all of the support she has always received from them.

Last, I would like to thank my husband Brandon for holding us together though the moments when time is scarce and stress is high, also for his support, love, and care.

# TABLE OF CONTENTS

# LIST OF FIGURES

# LIST OF TABLES

# LIST OF NOMENCLATURE

| | | |
|---|---|---|
| $B$ | = | Baseline |
| $C1$ | = | Contour #1 |
| $C2$ | = | Contour #2 |
| $C_x$ | = | Axial Chord [m] |
| $C_P$ | = | Specific Heat at Constant Pressure [J/kg] |
| $Cp_T$ | = | Total Pressure Loss Coefficient |
| LE | = | Leading Edge |
| $\dot{m}$ | = | Mass Flow Rate [kg/sec] |
| MF | = | Purge Flow as a Percentage of Mainstream Flow |
| MC | = | Mid Chord |
| $\eta$ | = | Efficiency |
| P | = | Pressure [Pa] |
| RANS | = | Reynolds-Averaged Navier-Stokes Equations |
| s | = | Entropy [J/kg/K] |
| $T_q$ | = | Torque [N m] |
| TE | = | Trailing Edge |
| U | = | Rim Speed [m/sec] |
| $V$ | = | Flow Velocity [m/sec] |
| $V_\theta$ | = | Flow Velocity in the Circumferential Direction [m/sec] |
| $\omega$ | = | Rotational Speed [rad/sec] |

| | | |
|---|---|---|
| $M$ | = | Mainstream Flow Subscript |
| $P, s$ | = | Purge Flow Subscript |
| $o,T$ | = | Stagnation Quantity Subscript |

# CHAPTER ONE:
# INTRODUCTION

## 1.1 Introductory Remarks

In the approach to increase gas temperatures for better efficiencies in gas turbines, components must, in change, be cooled. Therefore, gaps in between rotating and stationary components are supplied with air to avoid ingress of hot gas. However, when the coolant ejects into the main flow, it enhances the secondary flow loss mechanisms already encountered in the mainstream flow. As a result, it becomes relevant to understand how these losses are generated and to investigate how they can be controlled.

This study focuses on the aerodynamic impact that the purge flow incurs on the turbine's main gas path. In order to reduce this impact on loss, the study proposes a platform design in the circumferential direction that could pump the flow out into a desired region, to reduce the suction side of the horseshoe vortex, so that it remains close to the wall to reduce loss. Additionally, if the purge flow is manipulated, it could incur more cooling in the platform at less pressure penalty.

## 1.2 Research Objectives and Methods

While researching purge flow interaction with the secondary flows it was evident that there was a need for manipulating the secondary flows. Therefore, the location at which the purge flow

exits the cavity and enters the mainstream flow is relevant. This surfaced the objective of researching a method of controlling the behavior of the purge flow. As a result, the objective of this work is to present a geometrical way, by which the flow is relocated, and therefore produces reduced loss. The idea is to contour the platform near the rim seal in the circumferential direction.

In the upcoming chapters, the design of the geometry, the methods and computations, and the result of this proposal will be discussed. Therefore, the overall objective of this project is to reduce aerodynamic losses in a turbine stage, and through computations, it will become evident if this goal was achieved.

The method used to accomplish this goal is Computational Fluid Dynamics. Therefore, this study is strictly computational but demonstrates trends that occur in a realistic turbine environment. Additionally, two geometries will be presented against a baseline case at different swirl conditions and mass flow rates.

## 1.3 Thesis Overview

In this work the main research will be introduced in chapter one. In chapter two, the literature review will be presented so that the reader can achieve a better understanding of concepts that lead to the thesis presented in this work and assessments of how this new idea could improve the current designs. Chapter three has an exhaustive explanation of the methods used in this work. Chapter four provides the results and a discussion of the results from the recent study. Lastly, chapter five resumes the work and concludes the main results. It also provides recommendations for future work.

# CHAPTER TWO:
# LITERATURE REVIEW

In the last decade, targeting the major causes of aerodynamic loss has become one of the prime focuses of turbine designers. The profile loss, which occurs due to the boundary layer formation, is a small percentage of the total aerodynamic loss in a turbine. Therefore, it is relevant to study and understand the other sources of loss so that they can be targeted and potentially reduced.

This chapter contains a summary of the studies and findings relevant to this study. First, a discussion on secondary flows will be presented. Second, endwall contouring findings will be explored. Third, research on purge flow will de discussed. Lastly, a combination of both endwall contouring and purge flows will be assessed in order to demonstrate the importance of considering both during analysis, and last, a new idea will be proposed with the purpose of improving the aerodynamic performance of the first stage of the engine.

## 2.1 Secondary Flows

One of the major impacts in efficiency loss in turbines can be attributed to secondary flows. These flows are composed of three-dimensional rotation which impacts the main flow two-dimensionality.

Understanding the secondary flow structure is the first step into controlling and reducing loss. Secondary flow is responsible for about 33%of the estimated total aerodynamic losses in a stage (Denton, 1993). Sieverding (1985), Langston (2001), and Wang et al. (1997) provide

explanations of the structure of secondary flows. Their explanations and studies show how the boundary layer encounters the high pressure from the leading edge of the blade and separates into the horseshoe vortex. However, in the paper, "Flow Visualization in a Linear Turbine Cascade of High Performance Turbine Blades" Wang et al present an experimental study of the structure of secondary flows in a turbine stage. This structure is shown in Figure 1 and is used as a basis for this study.

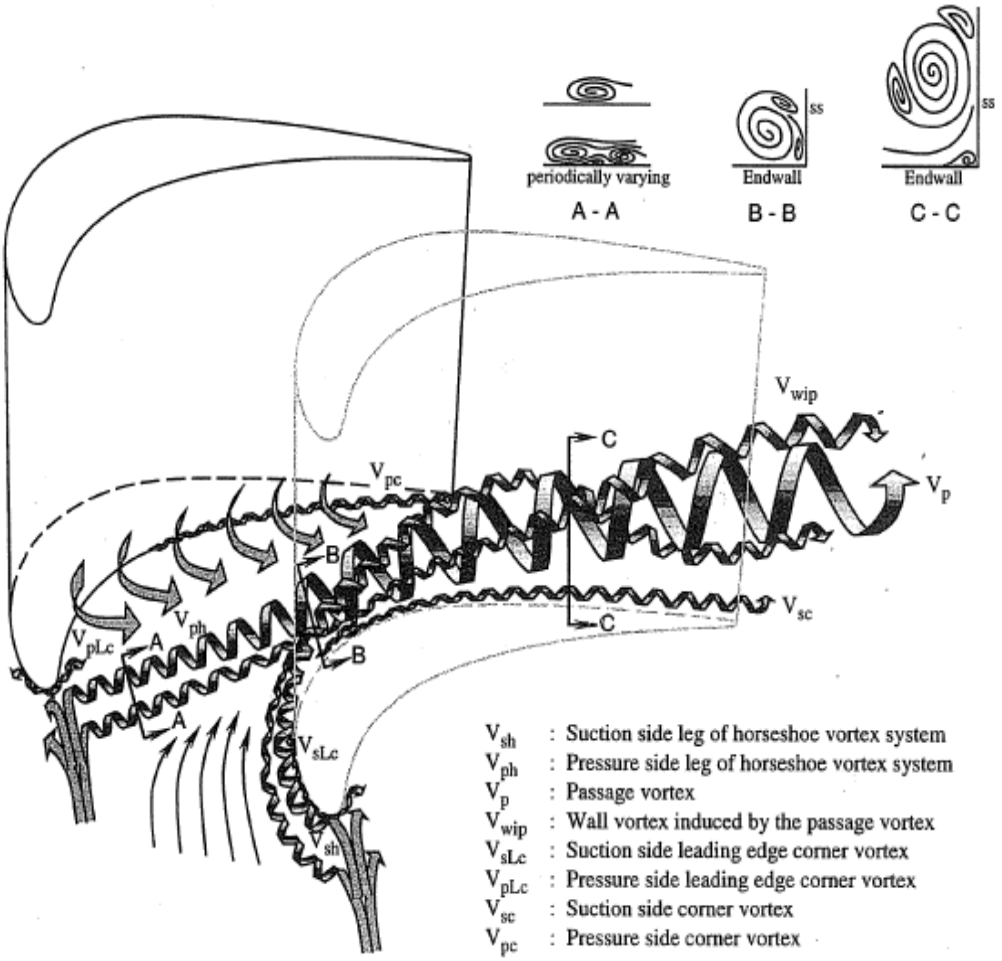


**Figure 1: Secondary Flow Structure (Wang et al., 1997)**

The secondary flow structure presented in Figure 1 was achieved through a flow visualization technique. This demonstrated that there was a clearer understanding of secondary flow behavior, which is very complex by nature. By observing Figure 1 it can be deduced that secondary flows one main source. This source is the boundary layer formation at the inlet. This boundary layer grows in the axial direction until it reaches a disturbance (high pressure gradient). The main disturbance is the blade. The interaction of the boundary layer and the blade's pressure total gradient produces rotation in the flow which is conductive to vortex formation. Since the flow goes around the blade, two vortices are formed, one on the suction side and one on the pressure side. The pressure side vortex is swept by the cross flow, which is generated by the pressure gradient between the blade's suction side and pressure side. At about mid-chord, the suction side leg becomes entrained by the pressure side leg and they form the passage vortex. Additional vortices also occur because of the low momentum fluid from the end-walls interacting with the main flow. Some of these vortices get entrained in the passage vortex as well. However, the corner vortex, named this way due to the low momentum fluid at the mid-chord between the hub and the blade, remains low throughout until the stage exit.

The main loss generator is the passage vortex. This vortex generates about 15% of the aerodynamic losses in a stage. However, this is due to its formation because most of the vortices get entrained into this larger vortex. Thus, it is relevant to observe the cause of each of the vortices forming the passage vortex and possibly modify their development to decrease the overall passage vortex loss.

Another method to visualize the secondary flows close to the hub was presented by Benner et al. (1997). Figure 2 shows how the flow experiences several separation lines demonstrated by the

streamlines. A relevant point is R1 which shows there is a saddle point at the location of the horseshoe vortex. This technique will be used in the analysis of this study.

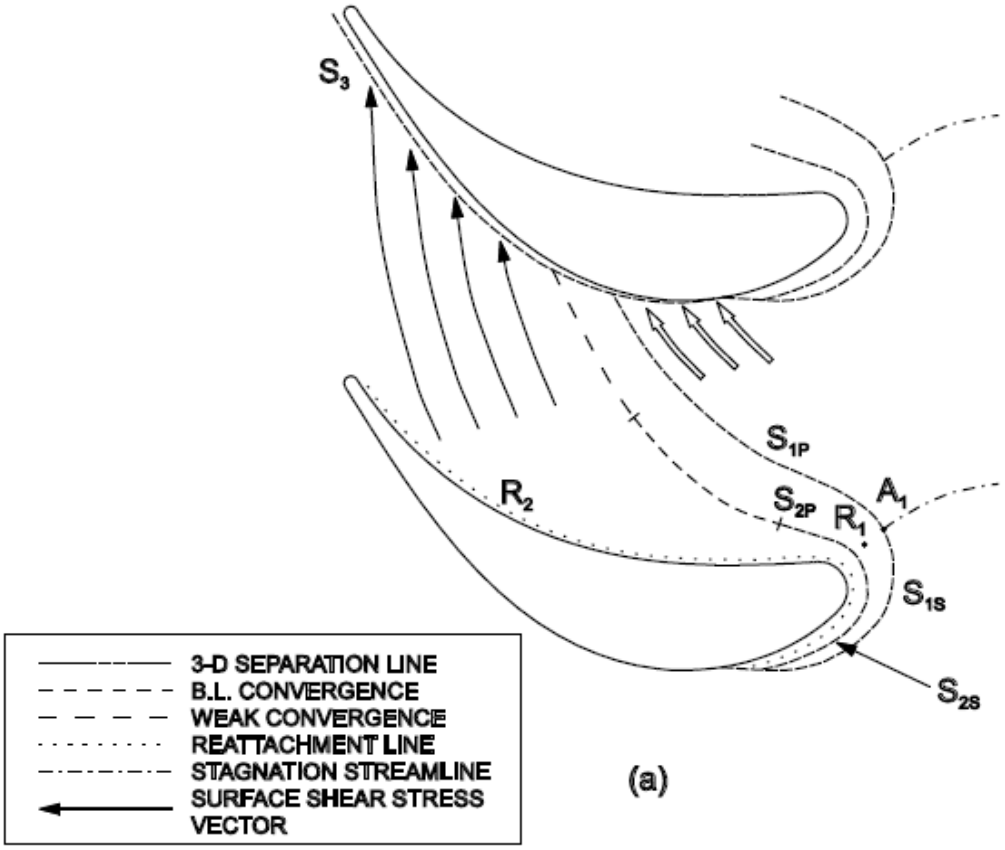


**Figure 2: Streamline Visualization at the Hub (Benner et al., 1997)**

## 2.2 Endwall Contouring

A way of manipulating secondary flow is by contouring the platform endwalls. This concept was first introduced as 2-D axisymmetric end-wall variation. Several geometries were tested

with no success because the areas that decreased loss affected the flow to the extent that it generated loss downstream, offsetting the overall benefit. Rose (1994) introduced the concept of "Non-Axisymmetric End-Wall Contouring" in the attempt to reduce end wall coolant by creating a homogeneous pressure field at the end-wall. He conducted computational experiments and obtained successful results by controlling the pressure field in the circumferential direction. Harvey (2000) proposed an optimized geometry for the non-axisymmetric end-wall (Figure 3) and obtained significant reduction of secondary loss (34%). However, more recently Schuback et at. (2009) combined both purge flows and end wall contouring and observed that the overall benefit of contouring is offset by the purge flow. Therefore, purge flow must be considered when contouring an end-wall.

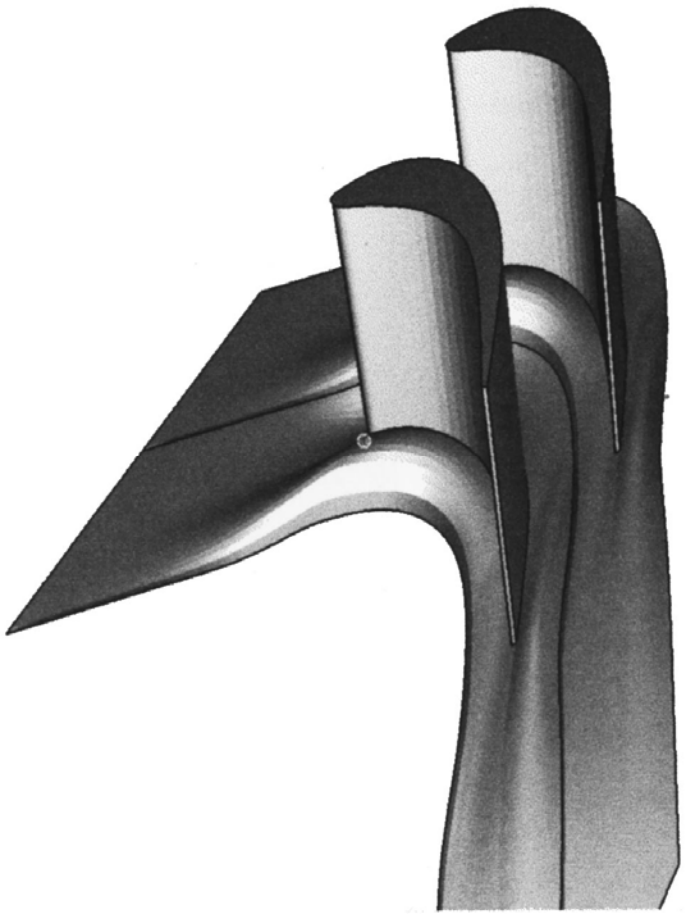

**Figure 3: Example of a Contoured Non- Axisymmetric End-Wall (Harvey et al., 2000)**

## 2.3 Purge Flow

Purge flow is flow used as platform coolant. This flow is bled from the compressor so that the coolant is relatively colder than the mainstream gas. Later, it is injected in the high pressure stage between the stationary and rotating components. Figure 4 shows the exit of the purge flow into the mainstream flow as it approaches the rotating blade. The gap in between the components leads to the rotor and hot air ingestion would be highly destructive to the part because at this location the parts generally have no thermal barrier coating for their protection. Therefore this air

is used as a coolant mostly to prevent hot gas from entering the platform seal. However, as mentioned previously, the purge flow gets entrained into the secondary flows and enhances losses. Because of this impact is that we consider purge flow as a method to control the secondary flow loss.

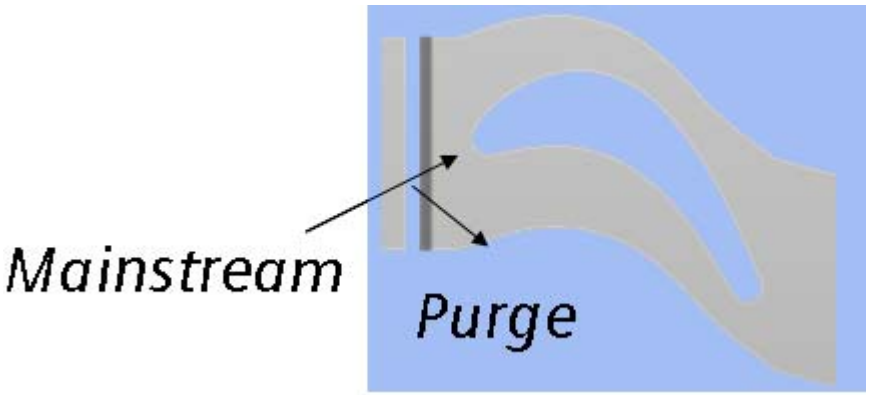


**Figure 4: Mainstream Flow and Purge Flow**

Purge flow is affected by many parameters. Some researchers have focused on looking at the impact of higher mass flow rates, others have looked at the gap width and geometry, and others have observed the effect of having a buffer cavity. Overall, the major impact of this flow on loss is directly related to the tangential component of velocity the purge flow carries at the moment when injected into the main flow. Reid et al.(2005, 2006), Demagne and Longley (2000), and Zlatinov et al.(2011) are only some among many who have performed experimental and computational experiments on both turbines and compressors on the importance of purge tangential velocity. When the flow ejects with a tangential component, it counteracts the cross passage pressure gradient which reduces the strength of the secondary flow. Girgis et al. (2002) increased the tangential component of the flow and found a direct positive impact in the turbine efficiency. Therefore, observing and performing experiments with different tangential velocities

is relevant to reducing loss. Additionally, looking at diverse mass flow rates of injection provides the designer with a more ample design space while also reducing loss.

Even though there have been many attempts to control the purge flow, no one has observed the effects of end-wall contouring in the circumferential direction of the cavity.

## 2.4 Platform Contouring

In this study, a computational model is prepared to simulate a turbine first stage (Figure 5) in order to evaluate the effects of platform circumferential contouring over the losses generated by secondary flows in the turbine. The objective of the contours is to manipulate the location and strength of the flow, thus to modify the patterns of the horseshoe vortex and the passage vortex. Predicted results deliver a new concept that could potentially reduce aerodynamic losses in a turbine stage. The design of the contours will be further explained in the following chapters. One example of the proposed contours appears in Figure 5.

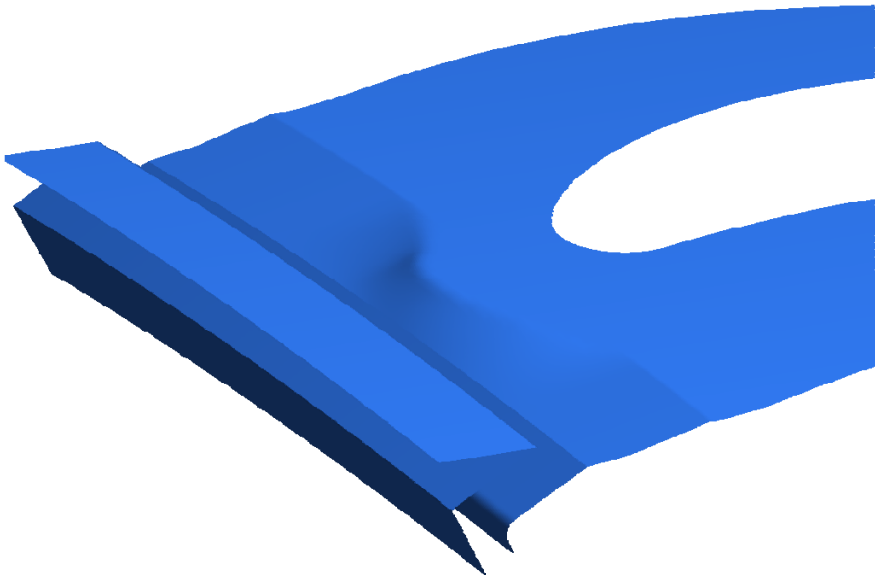

**Figure 5: Example of a Circumferential Contour (Contour #1)**

# CHAPTER THREE:
# COMPUTATIONAL METHODS

The model used for this study is comprised of a stator and a rotor, simulating a turbine first stage. The mesh contains 3.07 million grid points combined for both domains and y-plusses of less than 10 in most regions, and fewer than 7 in the most critical regions, which provides accuracy in the calculations. The y-plusses in the rotor domain can be seen in Figure 6. The computational technique used is three dimensional steady Reynolds Averaged Navier Stokes (RANS). The Turbulence model used in the computations is Shear Stress Transport (SST), which was selected because it resolves accurate calculations despite the complexity of the flow.

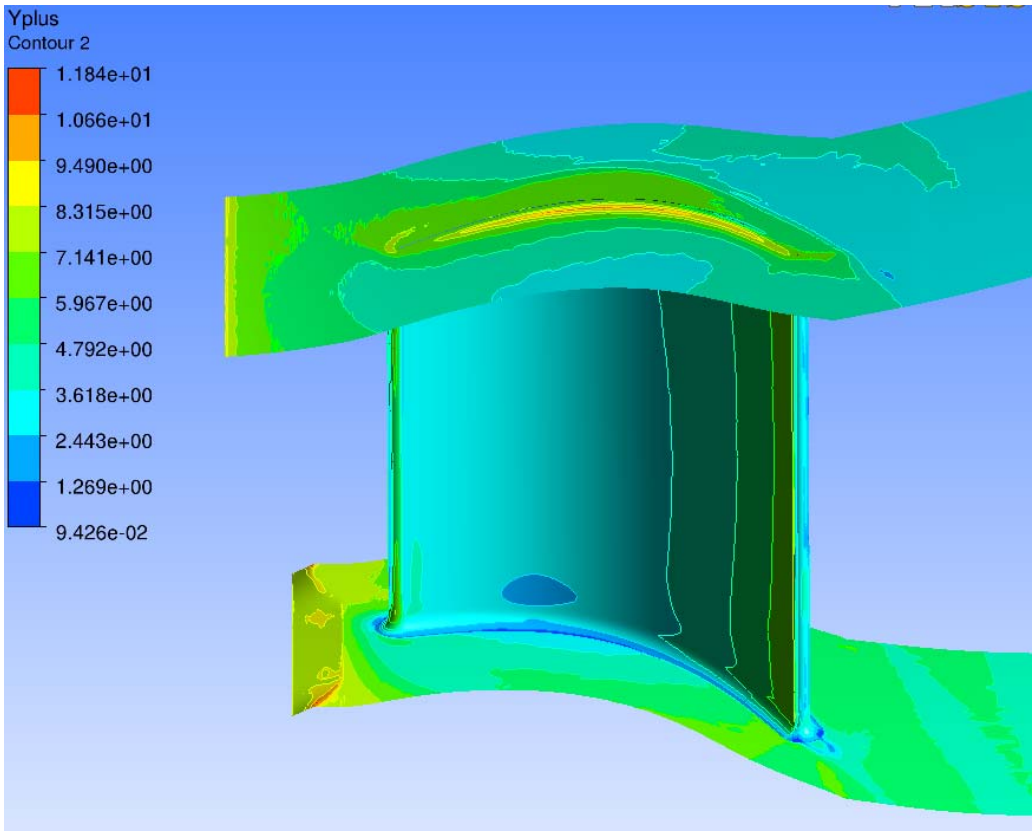


**Figure 6: Y plusses in Rotor Domain**

The domain has a cavity in between the stator and rotor, which in essence simulates the gap between the stationary and rotating platforms. The cavity is contained in the rotating domain, with a counter-rotating wall to simulate a stationary wall. Because the cavity is modeled with the rotor there is no mixing plane to average out the flow. The only location where a General Grid Interface (GGI) is located is between the stationary and rotating domains. This can be seen in below in Figure 7.

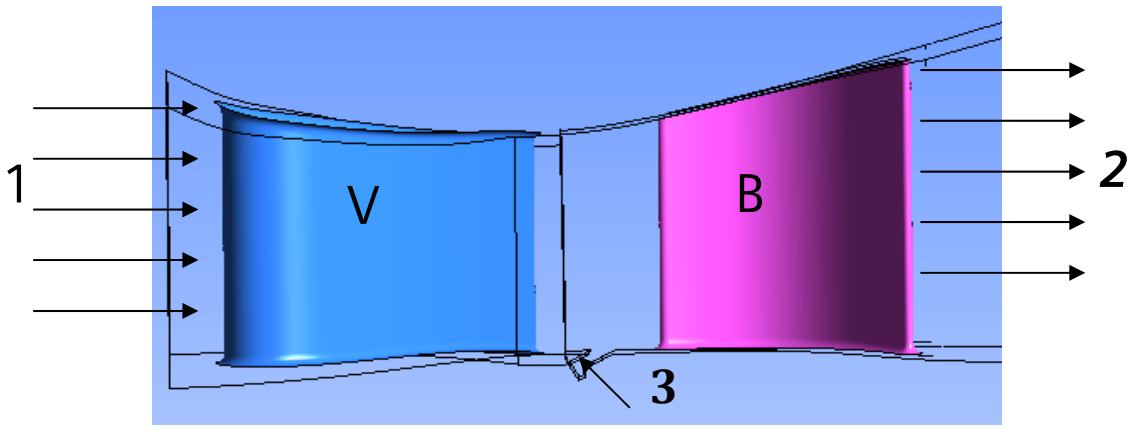


**Figure 7: Boundary Condition Location**

### 3.1 Boundary Conditions

As seen in Figure 7, there are three main boundary conditions. Condition 1 refers to the inlet of the mainstream flow (M) and it is determined by a total pressure, total temperature, and flow direction components to simulate a stator's outlet conditions. Condition 2 refers to the outlet of the mainstream flow which is defined by a static pressure. Condition 3 is located at the inlet of the rim seal (P). This boundary condition is defined by a mass flow rate that is a fraction of the inlet mass flow rate (0.5% or 1.5%). In order to indicate the amount of swirl, the tangential component of flow velocity is specified. These conditions are described in Table 1.

Table 2 shows the model's operating conditions, which are the same conditions as the ones used in Zlatinov et al. (2011) since the same model utilized for this study.

**Table 1: Boundary Conditions**

| ***M Inlet (1)*** | ***M Outlet (2)*** | ***P Inlet (3)*** |
|---|---|---|
| Ptotal (Po1) | Pstatic (P2) | Mass Flow Rate |
| Flow Direction Vectors | | Flow Direction Vectors ($V_\theta$ - swirl) |

**Table 2: Operating Conditions**

| Design Operating Point Data | |
|---|---|
| Flow Coefficient φ | 0.65 |
| Stage Loading ψ=Δht/U^2 | 2.17 |
| RPM | 2749 |
| U | 300 m/s |
| Rin Mach number | 0.759 |
| h/Cx | 1.11 |
| Tp/Tm | 0.518 |
| Reaction | 0.461 |
| $P_{trotorin}$ (Pa) | 525000 |

## 3.2 Parametrics

### 3.2.1 Cavity Geometry

In the process of generating the model, a simple cavity was selected. The geometry of this cavity represents a rim cavity overlap. The inner edge is rounded in order to avoid separation from a 90° turn. Additionally, the mesh is refined in the edges to capture all of the end wall effects with a 1.0 E-5 distance from the wall. Figure 8 shows the cavity geometry and the grid. The cavity grid changes in the circumferential direction as it adapts to the contours because they affect the grid points at the cavity-main flow interface.

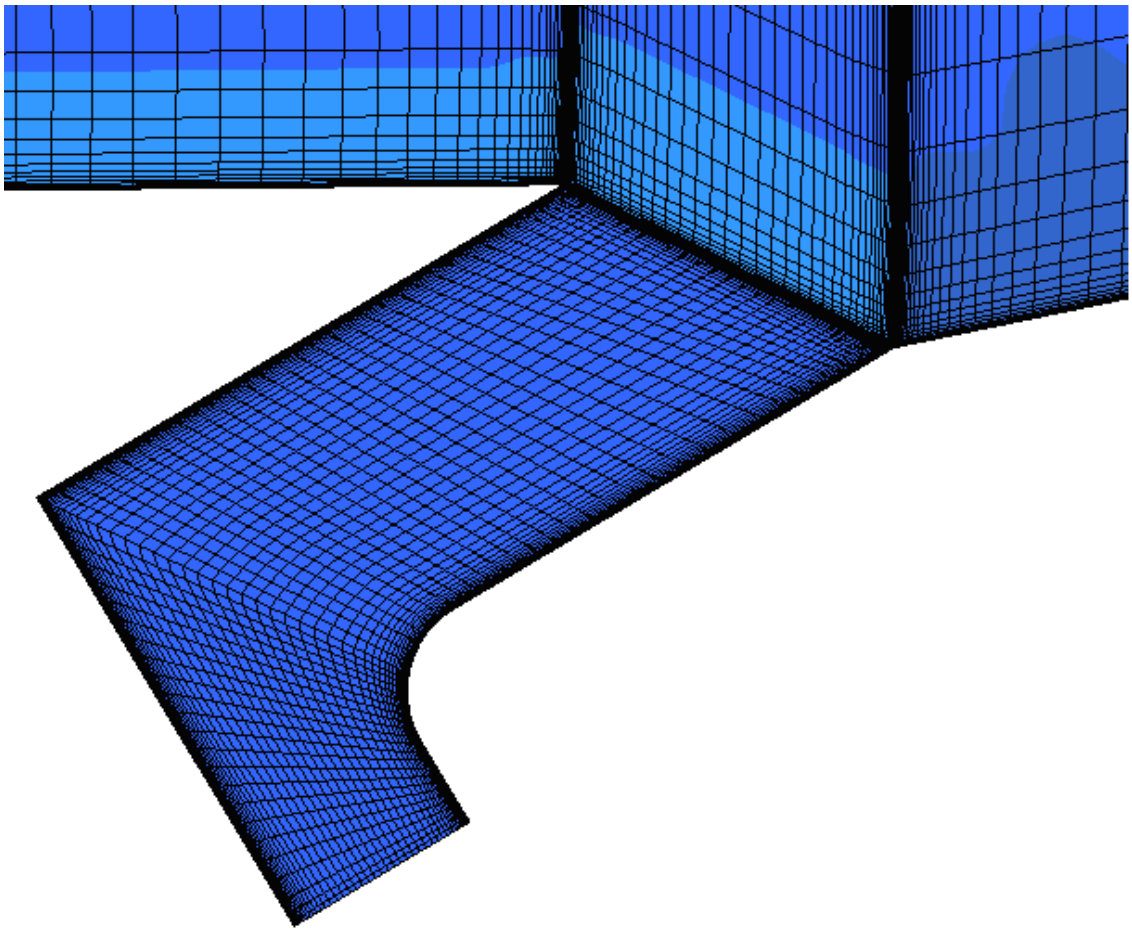

**Figure 8: Cavity Geometry**

### 3.2.2 Baseline and Contours

A baseline case was selected so that the contours can be compared to a generic rim seal design. The baseline, shown in Figure 9 a), has a cavity normal to the hub. It does not have a contour in the tangential direction but rather consists of a linear gap. Baseline computations will be performed at the same operating conditions as the contours so that it can be used as direct comparison. Contour #1 (C1) appears in Figure 9 b). The contour occurs in the circumferential direction at the rotating side of the hub-platform. Contour #2 has the same geometry of Contour #1, but it is offset one half a pitch (i.e. 2.8125°). This contour is shown in Figure 9 c).

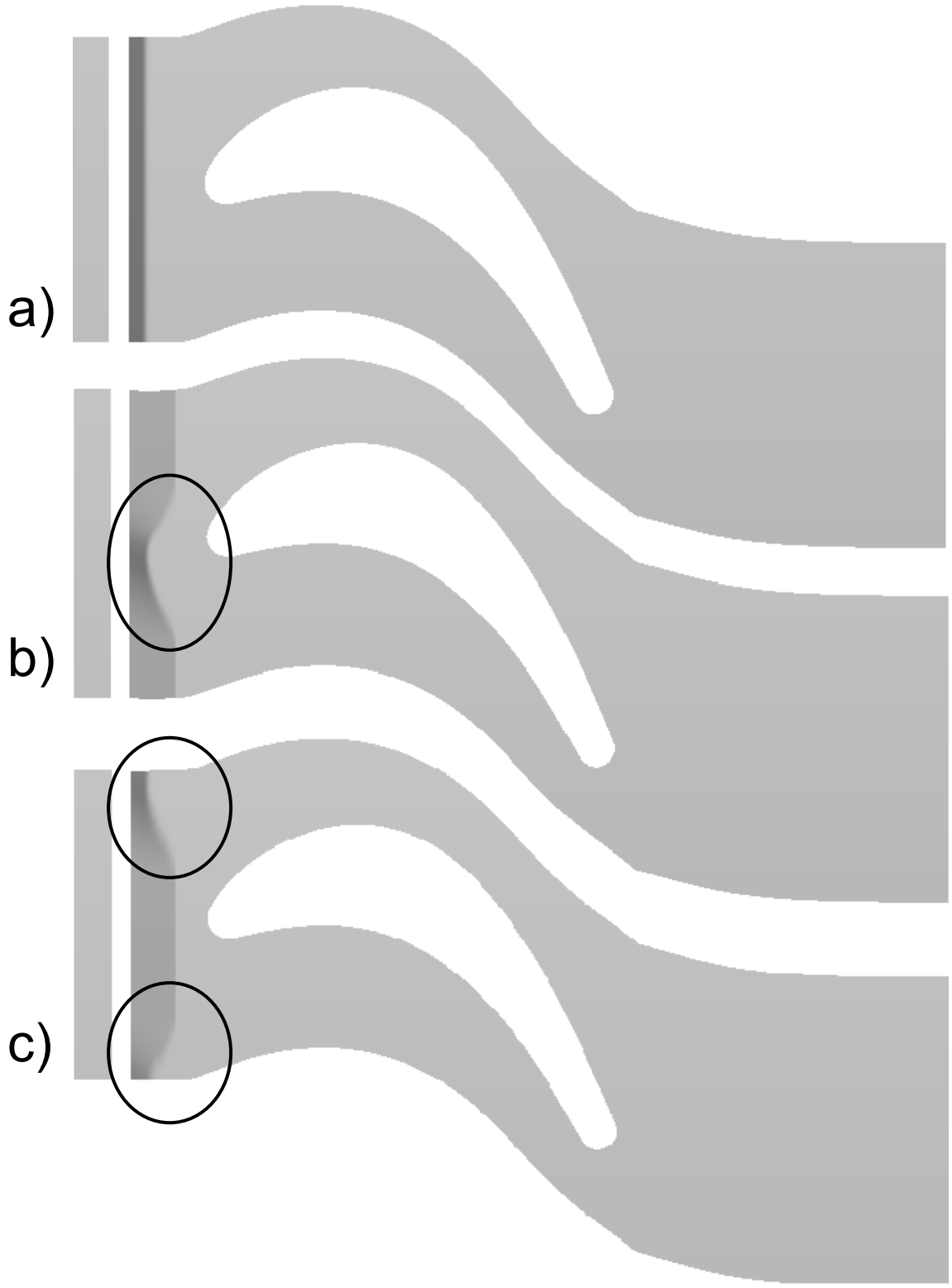


**Figure 9: a) Baseline b) Contour #1, c) Contour #2**

### 3.2.3 Test Matrix

The matrix shown below in Table 3, provides a perspective of the performed computations. This task will allow for ample, and in depth comparison of the major effects on the main flow generated by the contours. However, because the results from the computations at 1.5% MF are more pronounced than at 0.5% MF, but follow the same trend, the result at 1.5% MF will be used predominantly throughout this paper. Toward the end of the paper the results of the lower mass flow rate will be presented and analyzed so that designers of future engines can compare use the results more relevantly.

**Table 3: Test Matrix**

| | MF | Swirl |
|---|---|---|
| **Baseline** | 0.50% | 0% |
| | 0.50% | 50% |
| | 0.50% | 100% |
| | 1.50% | 0% |
| | 1.50% | 50% |
| | 1.50% | 100% |
| **Contour #1** | 0.50% | 0% |
| | 0.50% | 50% |
| | 0.50% | 100% |
| | 1.50% | 0% |
| | 1.50% | 50% |
| | 1.50% | 100% |
| **Contour #2** | 0.50% | 0% |
| | 0.50% | 50% |
| | 0.50% | 100% |
| | 1.50% | 0% |
| | 1.50% | 50% |
| | 1.50% | 100% |

## 3.3 Variables to Evaluate Vortex Location and Loss

Two variables were used in this paper to give clarity to the results: Velocity Stretched Swirling Strength, and viscous entropy generation. These variables will be explained with detail in this section.

### 3.3.1 Velocity Stretched Swirling Strength (VSSS)

It is hard to define a vortex core numerically based on the computed flow field. The magnitude of vorticity seems to be the most suitable parameter to use. However, vorticity is the measure of the rotational nature of, or shearing within, the flow field that will be identified, which may or may not correspond to a rotating fluid structure or a vortex. For this reason, several automated criteria have been developed over the last two decades, e.g. those proposed by Chong et al. (1990), Zhou et al. (1999), and Chakraborty et al. (2005).

In this work, a modified version of the criterion proposed by Zhou et al. (1999) is used. First, according to Chong et al. (1990) a vortex is represented by that region inside flow field where an Eigen-value pair of the velocity gradient tensor is complex. Following this work, Zhou et al.(1999) defined swirling strength as the magnitude of the imaginary part of this complex Eigen-value. This swirling strength can be taken as the "unambiguous measure of rotation" (Christensen and Adrian, 2002). "Stretched swirling strength is swirling strength times dot product of swirling vector and normal of swirling plane. An increase in this parameter indicates that swirling strength normal to swirling plane is increased."(Akturk and Camici, 2011) Therefore, the Velocity Stretched Swirling Strength can be plotted as a contour to show the locations where a vortex can be encountered in the flow through the intensity of the rotation.

### 3.3.2 Viscous Entropy Generation

Another parameter used is entropy generated due to viscous effects (Denton, 1993). This parameter is relevant to this study because it can present how the losses are generated at each axial location by accumulated loss. Additionally, it shows how the viscous losses impact the turbine performance. The study performed by Zlatinov et al. (2011) (Appendix B) contains explanation of how this formula can be used to measure accumulated loss. It discusses how this parameter can be related directly to work lost because the expansion is happening in a non-ideal turbine. Equation 1 shows how viscous entropy is related to the work lost due to viscous effects. The development of this equation is shown in Appendix B.

$$w_{visc\ loss} = \widetilde{T}_{t2}\Delta s_{visc} = \widetilde{T}_{t2}\left(\Delta s - \Delta s_{therm}\right) = w_{ideal} - w_{actual} = c_p\left[T_{t2}^{ma} - T_{t1}^{ma}\left(\frac{P_{t2}^{wa}}{P_{t1}^{wa}}\right)^{\frac{\gamma-1}{\gamma}}\right] \quad \textbf{(Ref. 2)} \quad \textbf{(1)}$$

# CHAPTER FOUR:
# RESULTS AND DISCUSSION

The contours proposed in this study will be analyzed based on their aerodynamic performance. The presence of the contours affects the way the purge flow comes out of the cavity and interacts with the main flow. In this section we will discuss the effects of the contours on the secondary flow, the total pressure loss locally, the effects of swirl on the contours, and the entropy generation as a measure of loss. The efficiency of the different models will be used to demonstrate the overall behavior of adding the contours to the platform.

## 4.1 Secondary Flow Structure

It is relevant to observe how the contours affect the secondary flow structure because, as mentioned above, it is responsible for generating about one-third of the losses in a stage.

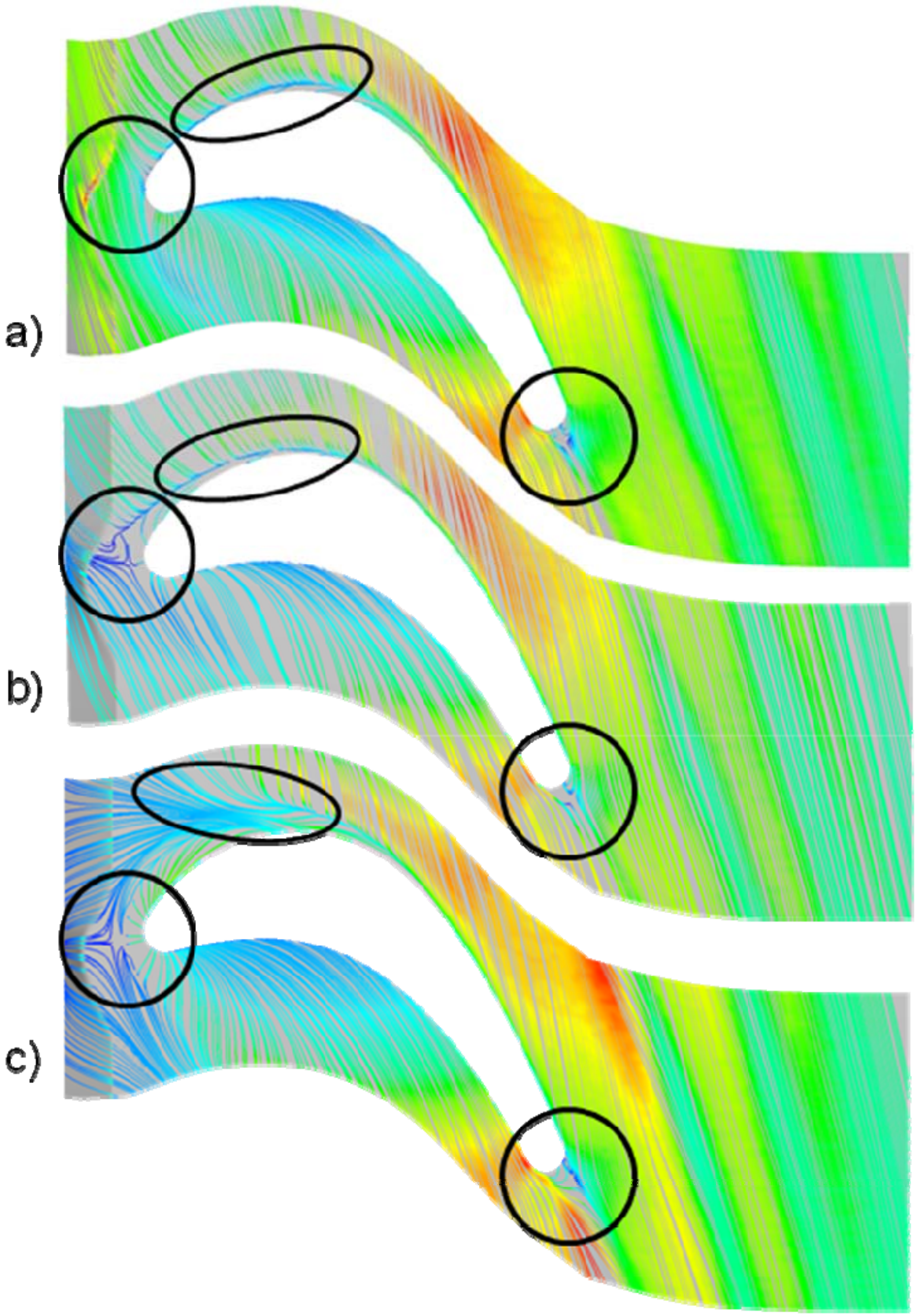


**Figure 10: Secondary Flow Structure at Hub of C1 with Changing Swirl a) 0% SW, b) 50% SW, and c) 100% SW**

Streamlines close to the hub are a great way of showing the secondary flow structure at the hub. Because the secondary flow structure is affected by purge flow, one can follow the path of the vortex formations. Inserting swirl to the cavity flow has shown to have a significant effect in reducing the losses. This can be seen in Figure 10 by looking at the streamlines at the hub of Contour #1. When the purge flow has been swirled, it does not promote the cross flow which in turn creates a vortex with less strength and at a lower span. This effect occurs at the proximities of the leading edge. When looking closely at the leading edge region of Figure 10 a), b), and c) it is clear that the swirl has a high impact on the structure of the flow at the suction side. It can also be seen in Figure 10 that the flow is affected all the way downstream until it reaches the trailing edge.

Because the secondary flow changes with the purge flow, it can be assumed that the purge flow can be used to control the secondary flow. Therefore, contouring the circumferential direction of the rotating platform could improve the overall performance of the engine reducing the effects of the secondary flow.

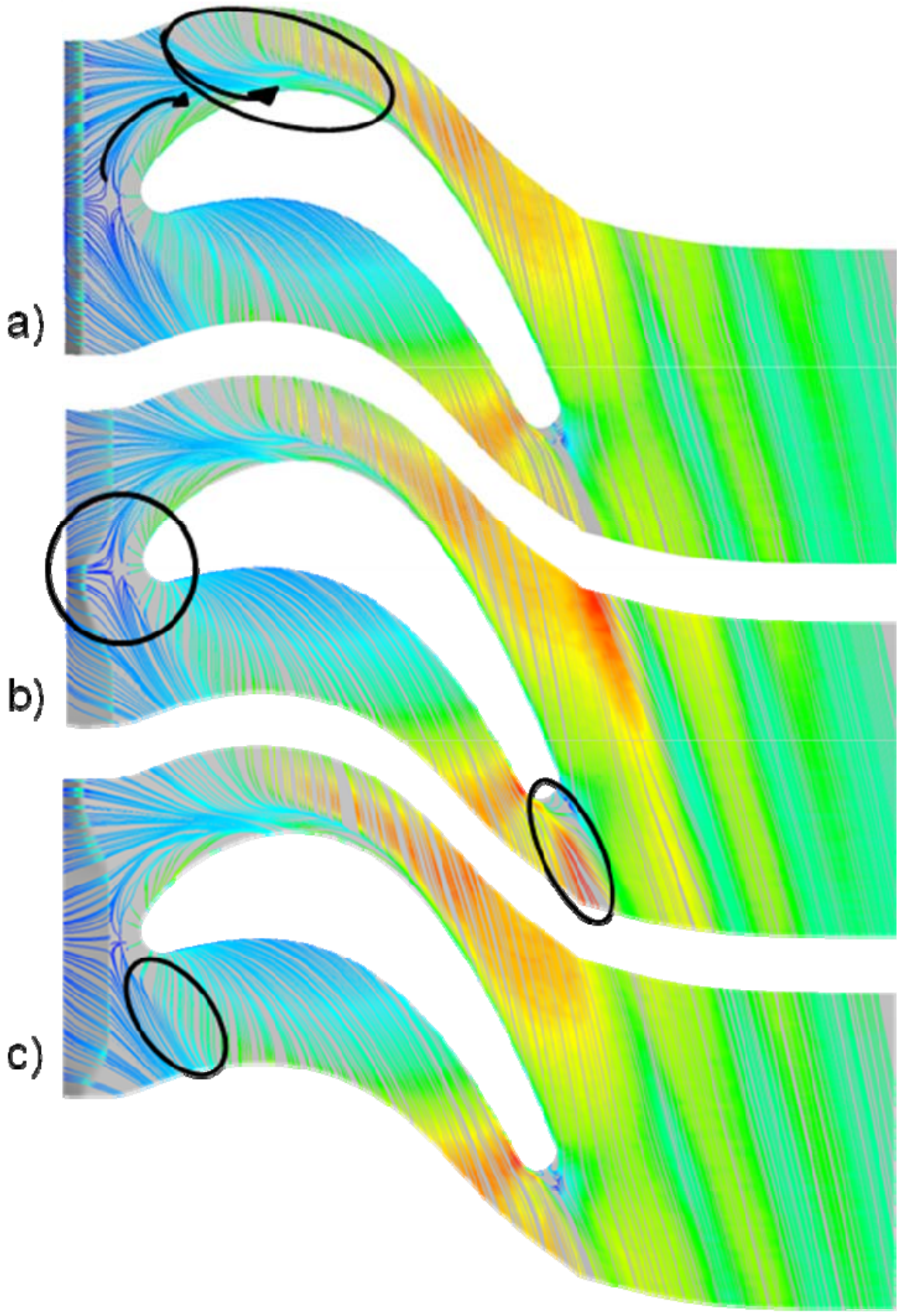


**Figure 11: Comparison of Secondary Flow Structure on Hub of a) Baseline, b) C1, and c) C2 at 100% swirl**

When the contouring is done on the platform, the local static pressure changes, therefore the flow is swirled locally. Figure 11 shows the comparison between the Baseline, Contour #1 and Contour #2. In this figure, Contour #1 is clearly changing the structure of the secondary flow by manipulating the flow. This contour reduces the cross flow. Additionally, Figure 11 b) shows that at the trailing edge, the wake is significantly smaller and streamlined, which demonstrates that the flow is experiencing fewer loss throughout the passage. Figure 11 c) reveals the effect Contour #2 has on the secondary flow. Because the flow exits at a different location, the saddle point has a different structure. This gives evidence to migrated flow and a possibility that there is more loss generated by this contour. The streamlines present one view of the secondary flow formation, however, more in depth analysis is presented below.

### 4.2 Total Pressure Loss and Vortex Intensity

In order to demonstrate the effects of the contours over the main flow, Figures 12-20 will show a comparison between the flow at the leading edge, mid-chord, and trailing edge at three swirl conditions: 0%, 50%, 100%. The total pressure used as a reference is located at the inlet of the rotor. This pressure appears in Table 2 as $P_{Trotorin}$.

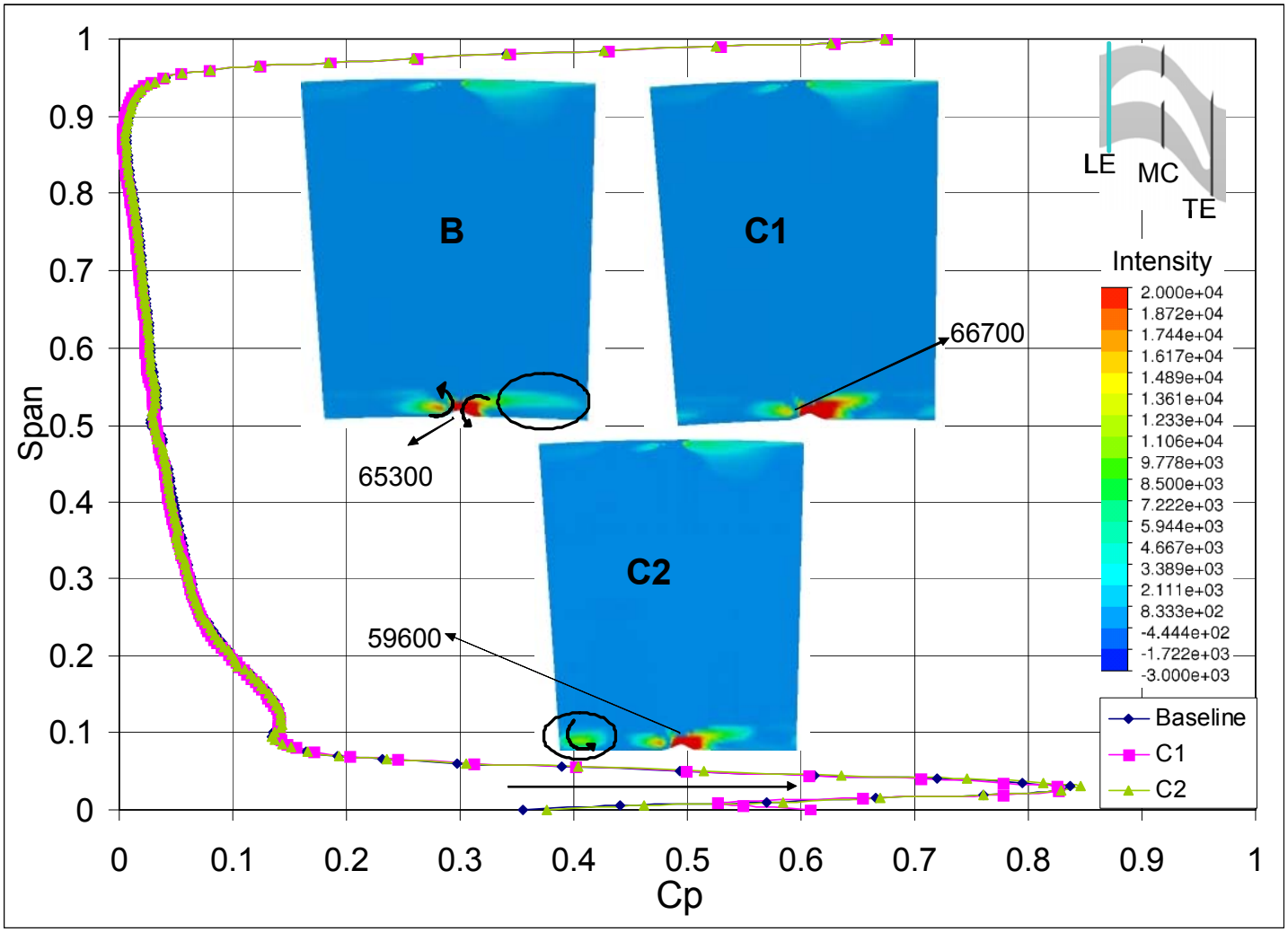


**Figure 12: Leading Edge Total Pressure Loss Coefficient and Vortex Intensity at 0% swirl**

It can be seen from Figure 12 that at the leading edge, the effects of having purge flow reach up to 9% span for all three contours. However, because of the impact of the contours, the flow behaves differently for every contour up to 9%. The effects can be seen more clearly through the vortex intensity (VSSS) contours. Figure 12 shows how the baseline at 0% swirl has two vortical structures. One of them is stronger than the other, but the effects carry on at the pressure side. On the other hand, Contour #1 has a more compact vortical structure that does not spread like the Baseline's structure. This vortex is also stronger with an intensity of 66700 (shown by the vortex intensity contour). Contour #2, has a structure similar to the Baseline, but with an additional vortex. Because the three contour plots are different, it is noticeable that the profiles do have an impact on the flow early in the development of the secondary flow (at the leading edge).

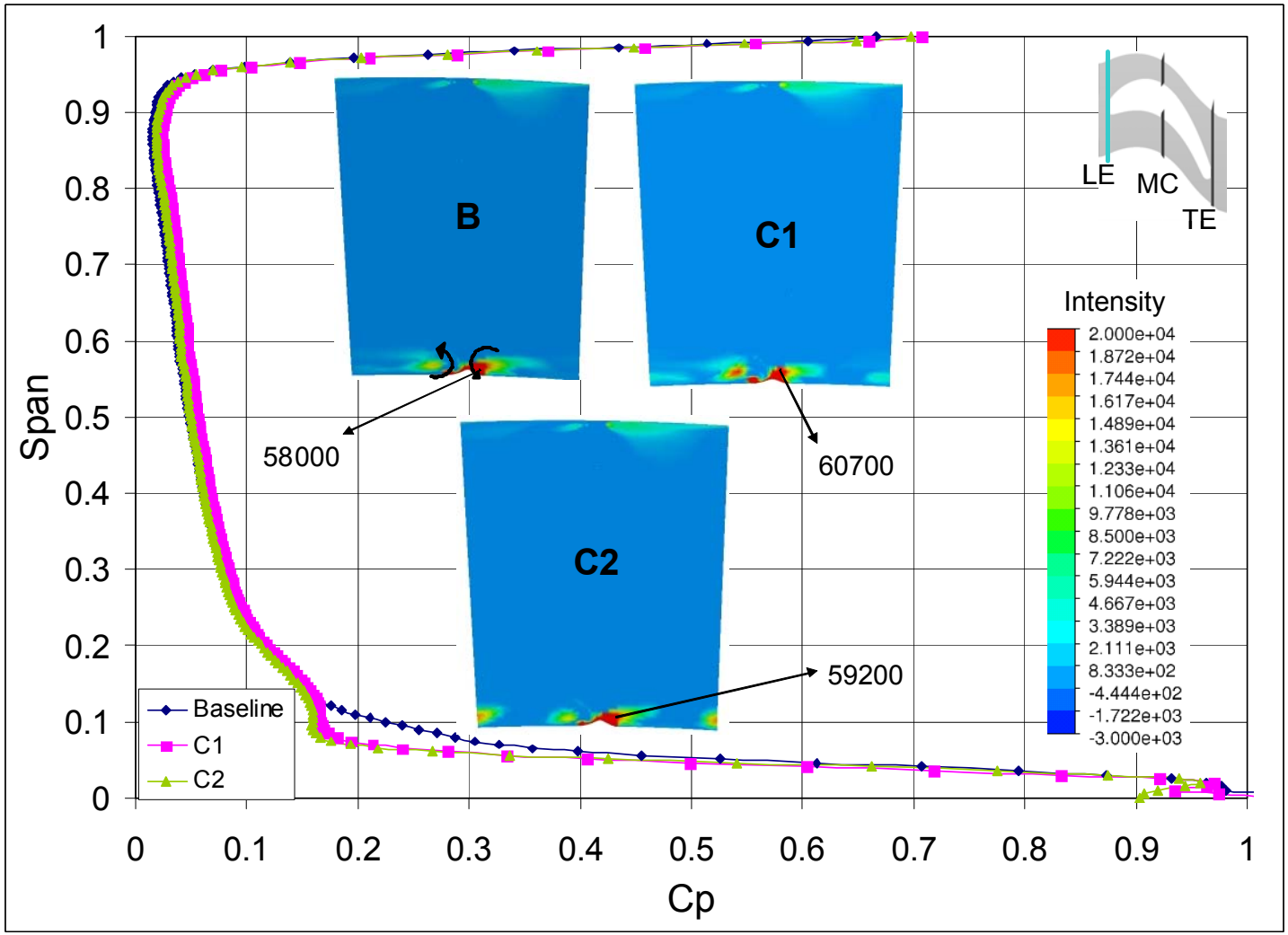


**Figure 13: Leading Edge Total Pressure Loss Coefficient and Vortex Intensity at 50% swirl**

The effects also change as the swirl changes. When the swirl is increased to 50%, the effects of the contours remain similar to 0% swirl with Contour #1 having the strongest vortex. This is shown in Figure 13. The strength of the vortices decreased for all three models when changing the swirl, which is also evident in the $C_{PT}$ plots as the loss increases closer to the wall.

When the swirl is increased to 100%, the structure of the flow changes and extra vortices are formed, with less strength and distributed within the 9% of the span. Figure14 also gives evidence of the distribution of the vortices through the contour plots. Also, because of the $C_{PT}$ loss plot, we can see that the loss is consistent at this location for the baseline and the two contours. Thus, at the leading edge the three contours resemble each other more than when fewer swirl is applied.

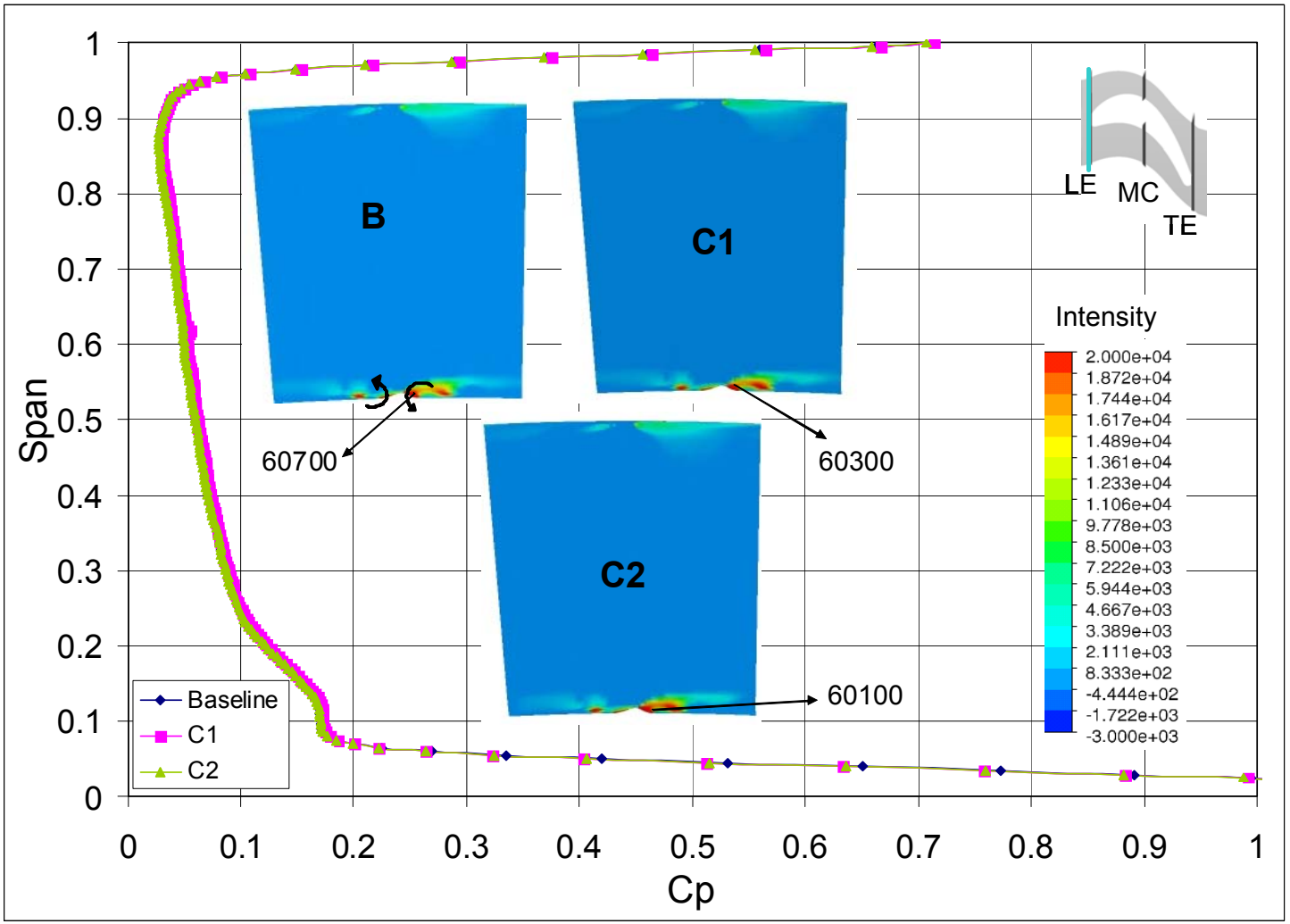


**Figure 14: Leading Edge Total Pressure Loss Coefficient and Vortex Intensity at 100% swirl**

More of the contours' effects can be seen at the mid-chord. The $C_{PT}$ loss plots show how the effects of the purge flow reach up to 30% chord but this decreases as the swirl is increased. Also, the passage vortex is developed and the core is located at about 20% span. In Figure 15 the $C_{PT}$ loss plots match with what is going on in the vortex intensity contours. The contour shows that the Baseline has the strongest vortex at the leading edge. It is also clear that the least intense vortex is at Contour #2 but it is split into two vortices of about the same intensity. However, one of the vortices is already at about 20% span at a high level of intensity, which means that the flow will experience increased loss downstream.

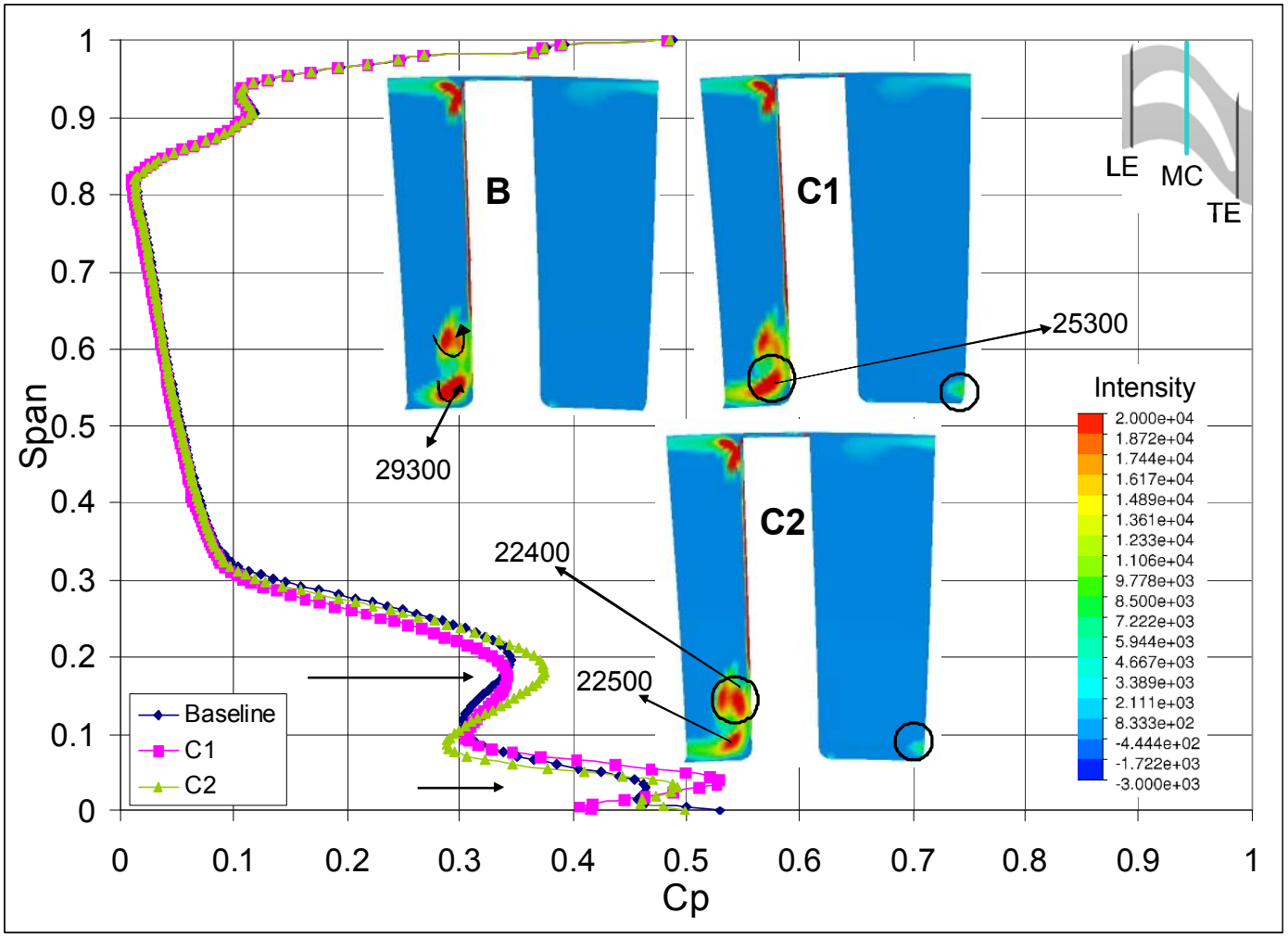


**Figure 15: Mid-Chord Total Pressure Loss Coefficient and Vortex Intensity at 0% swirl**

At 50% swirl the structure of the flow continues to be different from profile to profile. In Figure 16 Contour #1 seems to be the contour generating the least loss because the strongest vortex is still close to the wall with an intensity of 27100 (lower than the other two profiles). Contour #2 is still generating the most loss because the most intense vortex is at 20% span while the other two profiles have very low vortices. 50% swirl is the most realistic condition, thus it is relevant to notice that at this design point the contour with the best results is Contour #1. It is also pertinent to mention that 50% swirl is the most common condition found at the interface of the rim seal with the main passage, so this can be considered as the most relevant design point.

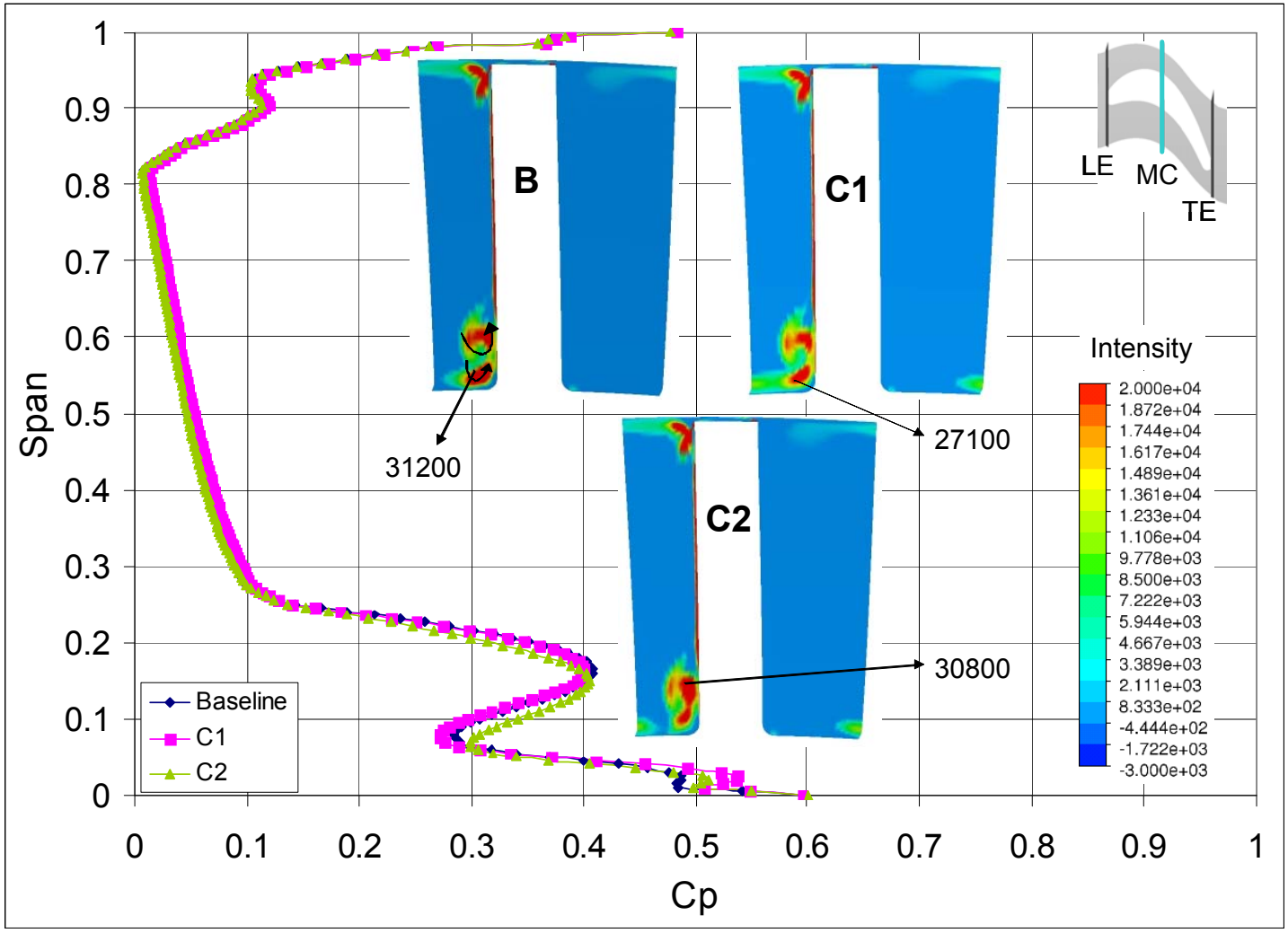


**Figure 16: Mid-Chord Total Pressure Loss Coefficient and Vortex Intensity at 50% swirl**

Figure 17 shows the effects of 100% swirl at mid-chord. At 100% swirl most of the vortex intensity contours resemble each other because they are located at about 10% span. However, the intensity shows us that the best candidate is still Contour #1, with an intensity of 39400. Because the difference in intensity between Contour #1 and Contour #2 is very small, clear conclusions can not be made at 100% swirl of which contour is performing the best. This behavior can also be seen in the $C_{PT}$ loss plots suggesting that at 100% swirl, the flow is not dependent on the wall geometry. However, one conclusion can be made, that is, at lower swirls Contour #1 has shown to be a better design.

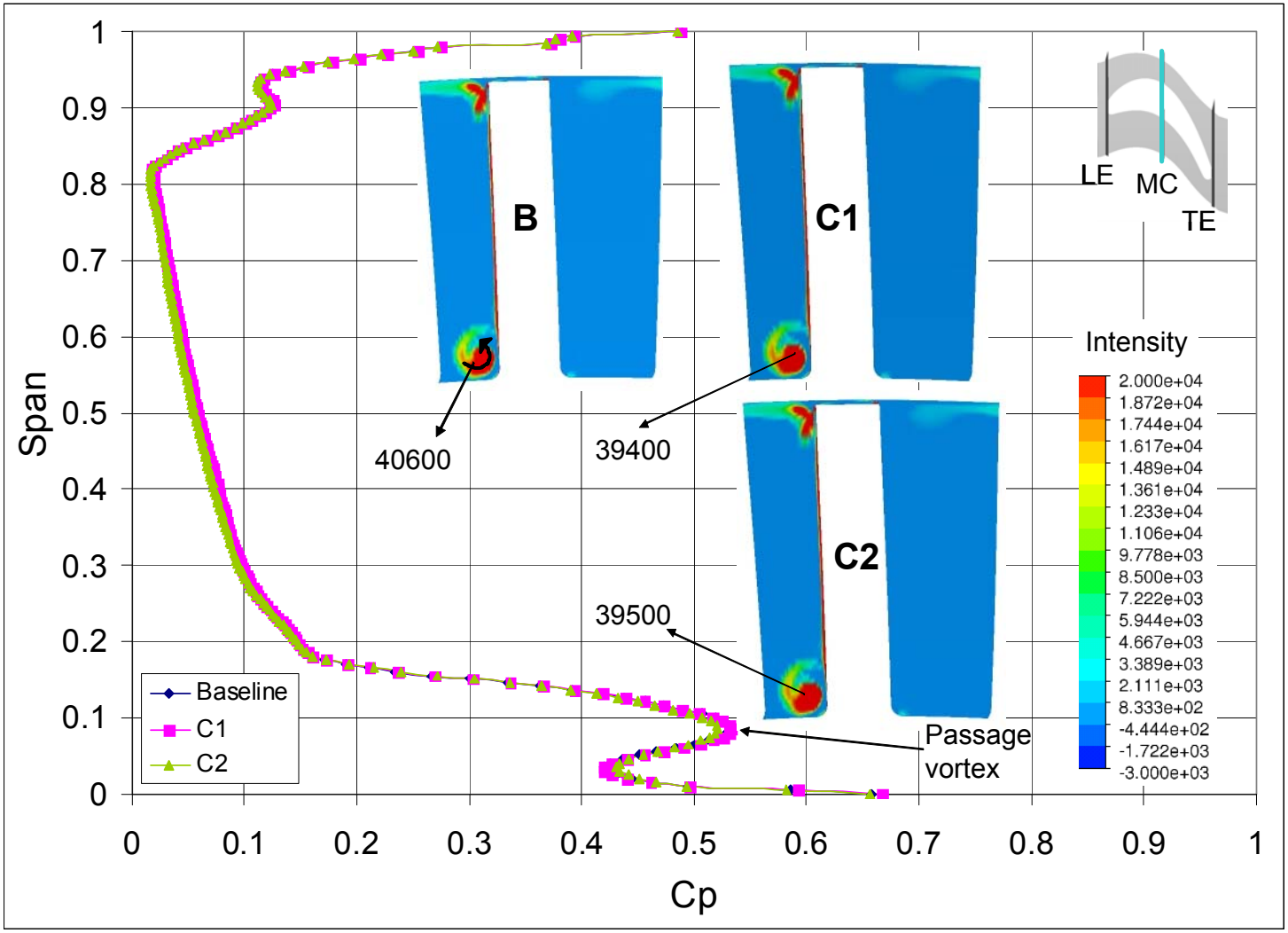


**Figure 17: Mid-Chord Total Pressure Loss Coefficient and Vortex Intensity at 100% swirl**

Figures 18-20 demonstrate that at the trailing edge there are only few differences that can be observed from contour to contour, but there are clear differences from swirl to swirl. The $C_{PT}$ loss plots show the location of the passage vortex core at 36% span for 0% swirl (Figure 18), at about 32% span for 50% swirl (Figure 19), and at about 25% span for 100% swirl (Figure 20). This marks a 10% difference in span (from 0%-100% swirl), which shows that at 100% swirl there is fewer loss because when the vortex remains low, the mid-span is free to extract more work from the main flow. Therefore, strong vortices, but close to the wall, generate less loss than weaker vortices closer to mid-span. Looking at the intensity one can notice that the lowest intensity for both the 0% swirl and 100% swirl is for the Baseline, but for 50% swirl Figure 19 shows that Contour #1 has the least intense passage vortex. This shows that Contour #1 has the best performance at 50% swirl for all three locations. For the lower swirls, it can still be deduced that Contour #1 has the lowest vortex with the least strength. Because the effects at the trailing edge show the overall impact, the author concludes that Contour #1 generates the least loss.

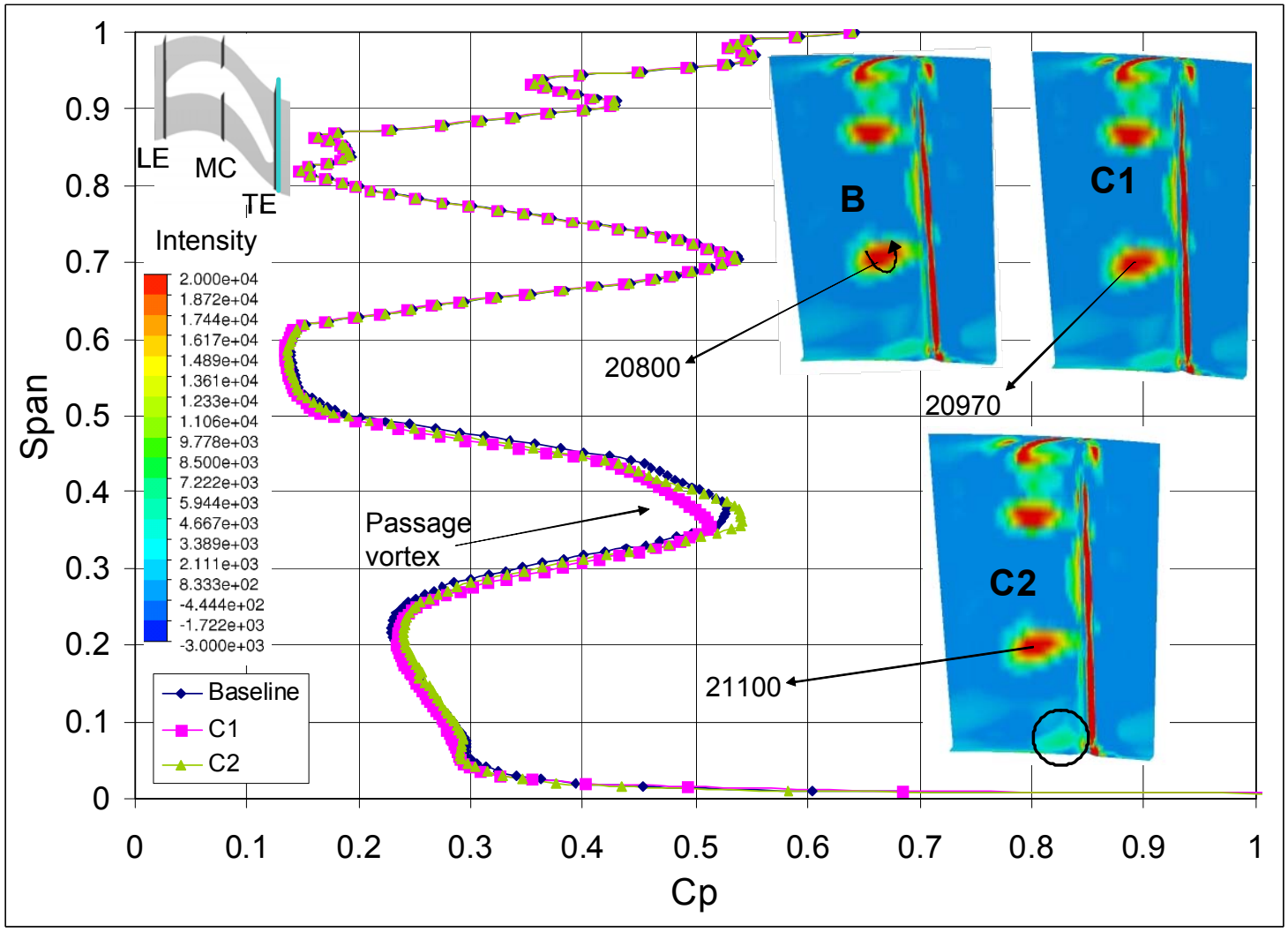


**Figure 18: Trailing Edge Total Pressure Loss Coefficient and Vortex Intensity at 0% swirl**

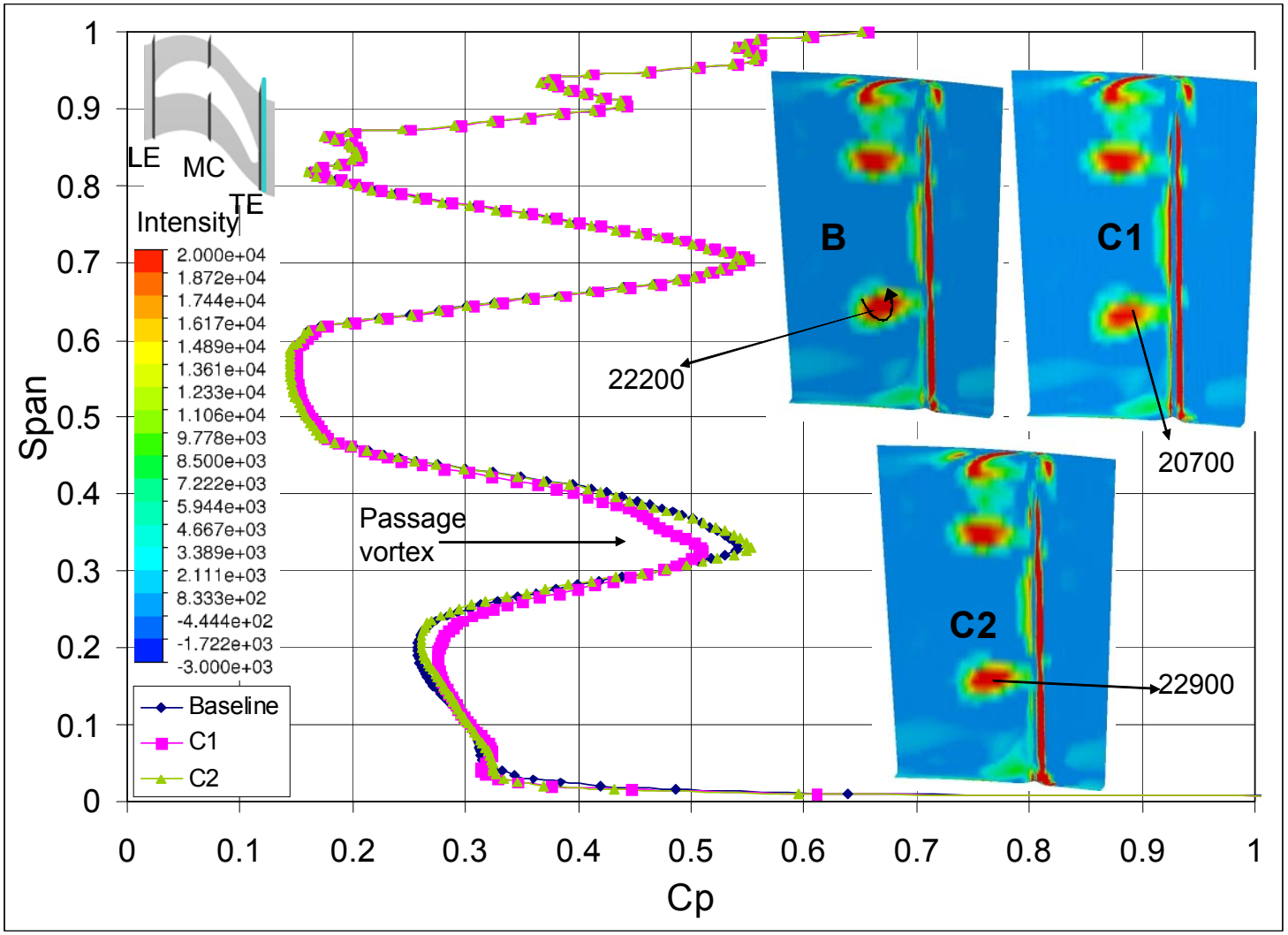


**Figure 19: Trailing Edge Total Pressure Loss Coefficient and Vortex Intensity at 50% swirl**

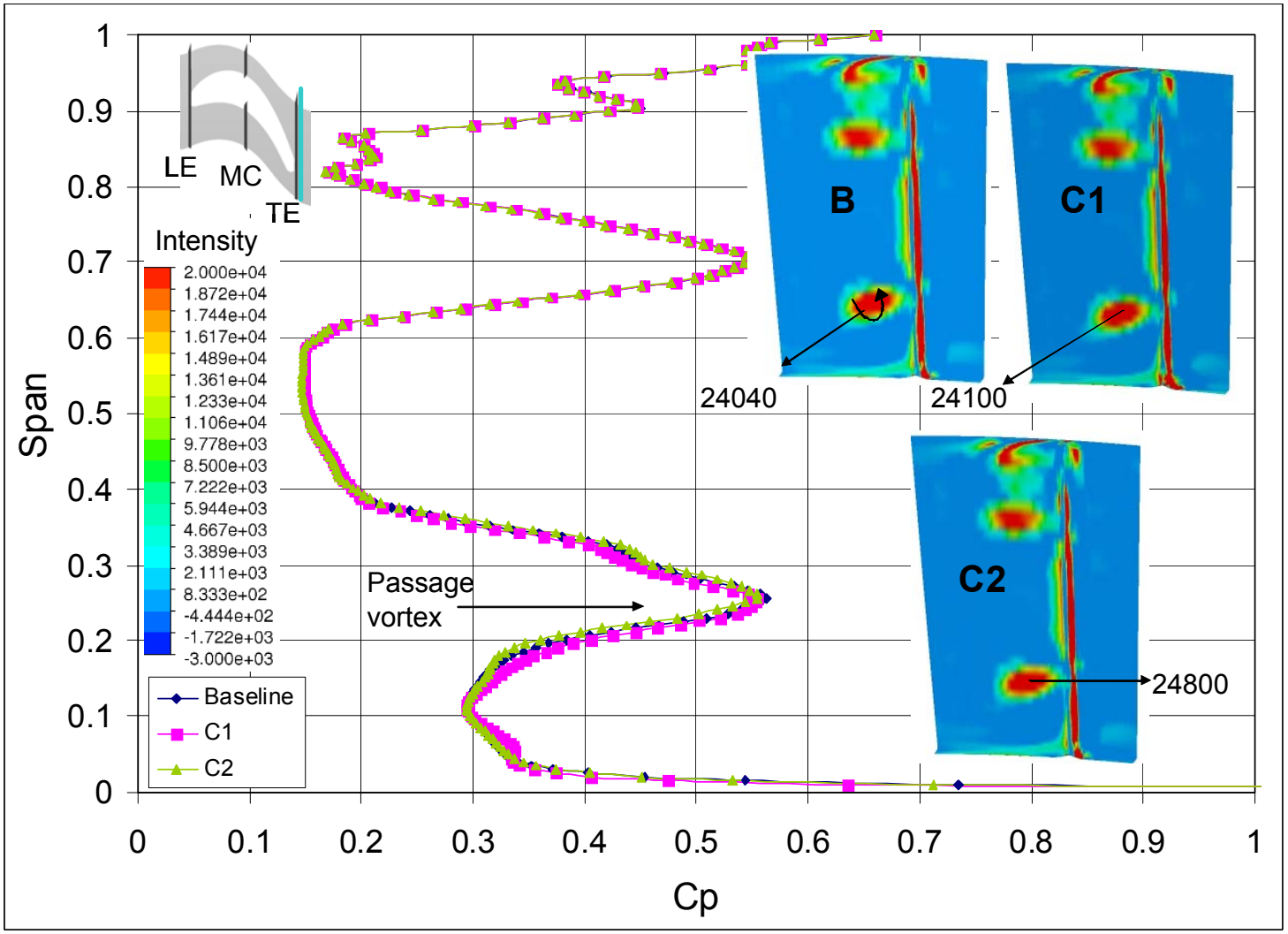


**Figure 20: Trailing Edge Total Pressure Loss Coefficient and Vortex Intensity at 100% swirl**

## 4.3 Vortex Control

The best way of visualizing a vortex is through plotting the isosurfaces of a vortex intensity level. Figure 21 shows the vortex formations of the Baseline and the two contours at 0% swirl. After the discussion mentioned above, it is more intuitive to observe the vortex behavior when plotted as an isosurface. Figure 21 shows how the purge flow exits at different locations. For the Baseline, the vortex exits at the pressure side but immediately gets transported to the suction side, where it gets entrained with the suction side of the horseshoe vortex at about 20% chord. The behavior of the purge flow is similar for both the Baseline and Contour #1. However, the entrainment occurs earlier (at about 15% chord). Furthermore, a large portion of the purge flow exits the cavity toward the suction side of the blade which gets entrained immediately with the suction side leg of the horseshoe vortex. This means that this contour would generate fewer loss as mentioned in the discussion above because the purge flow allows for the vortex to remain lower as it gets entrained earlier in the passage.

For the case of Contour #2, it is evident that the purge flow exits as two vortices, one at the pressure side, one at the suction side. Entrainment of these vortices occurs late in the flow (at about 50% chord) which hints that the losses are high and the passage vortex has lifted up because of the lack of strength from the purge to remain low (in span).

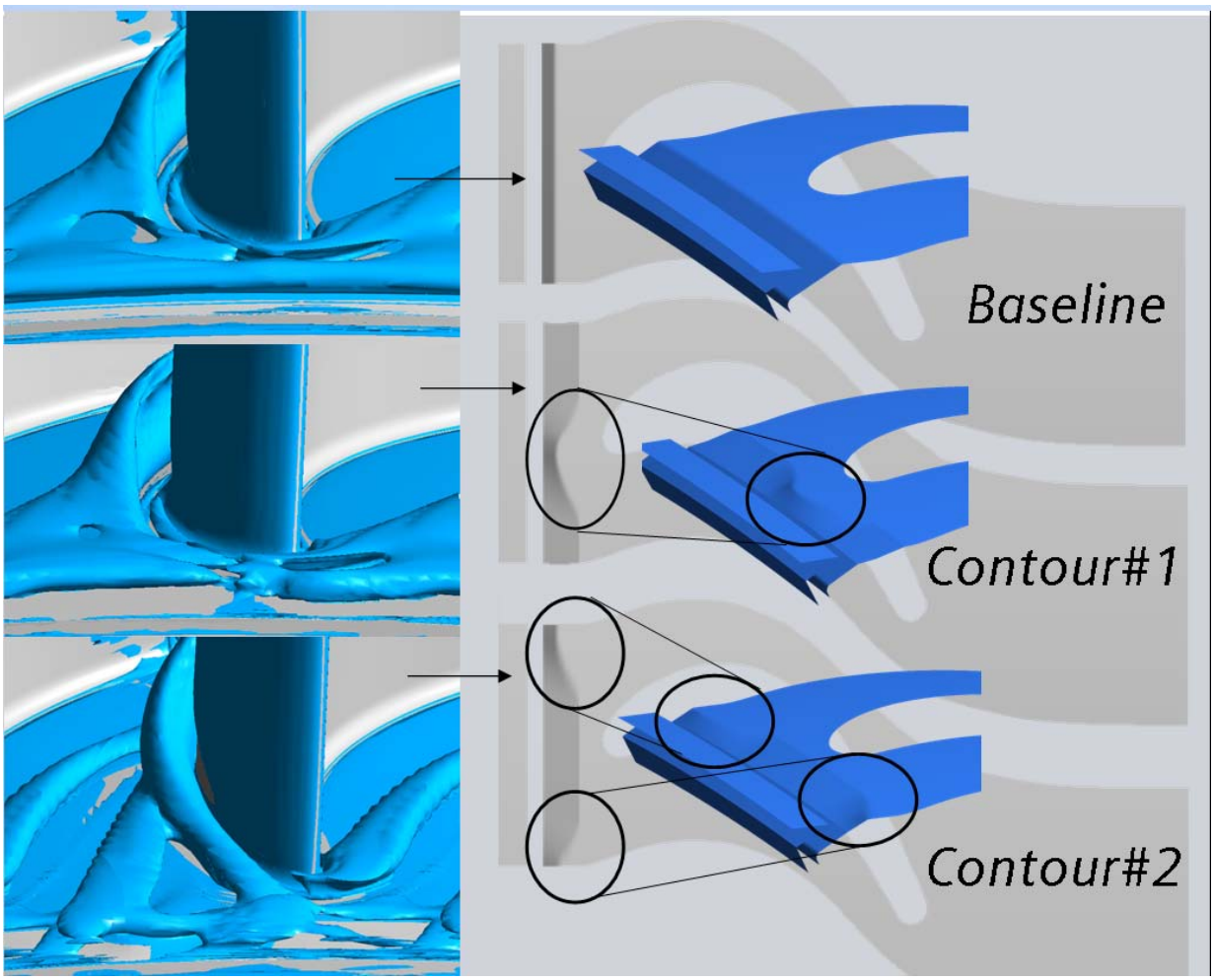


**Figure 21 Vortex Intensity Isosurface**

### 4.4 Swirl Study at Cavity Interface with Main Flow

A clearer picture of the effects of swirl becomes evident when observing the swirl locally at the cavity/main-flow interface. Figure 22 shows the percent values of the mass flow averaged swirl at the interface as the boundary condition changes from 0% to 50% to 100% swirl. The results obtained correlate to the results obtained earlier. Figure 22 shows how Contour #1 and Contour #2 have more swirl at 0% swirl and 50% swirl than the Baseline. This is because the

platform contours are swirling the flow locally, so when the results are mass averaged, the contours have more swirl than the Baseline. Even at 100% swirl, Contour #1 seems to swirl the flow more than the rest of the contours. This difference is very small, but because it is mass averaged it is convenient to observe the contours at the interface region (aligned with the hub). Figures 23 to 25 show the swirl locally at the interface.

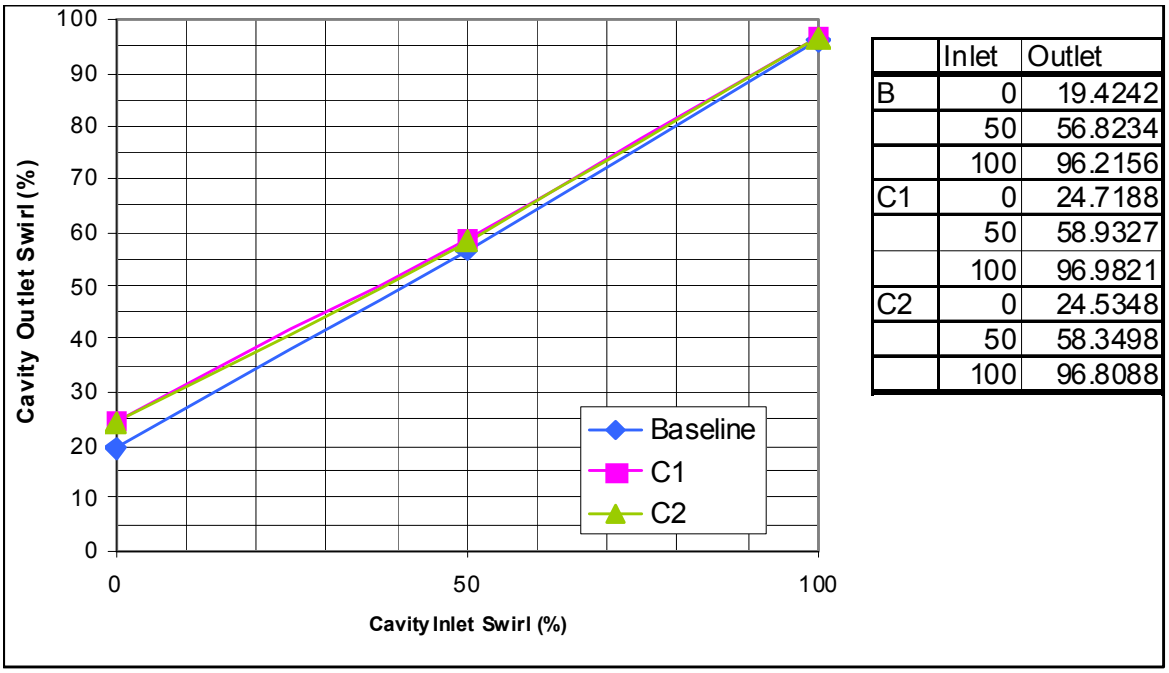


| | Inlet | Outlet |
|---|---|---|
| B | 0 | 19.4242 |
| | 50 | 56.8234 |
| | 100 | 96.2156 |
| C1 | 0 | 24.7188 |
| | 50 | 58.9327 |
| | 100 | 96.9821 |
| C2 | 0 | 24.5348 |
| | 50 | 58.3498 |
| | 100 | 96.8088 |

**Figure 22: Comparison of Percent Swirl at Cavity Inlet with Cavity Outlet**

The Baseline, shown in Figure 23, shows an even distribution of swirl for the 0% swirl. However, for the 50% case the distribution changes and fewer swirl gets picked up at the passage area. The 100% swirl case is affected by the static pressure distribution and more swirl gets picked up at the suction side of the blade. Higher swirl can be seen toward the suction side of the blade reaching values of over 100% swirl.

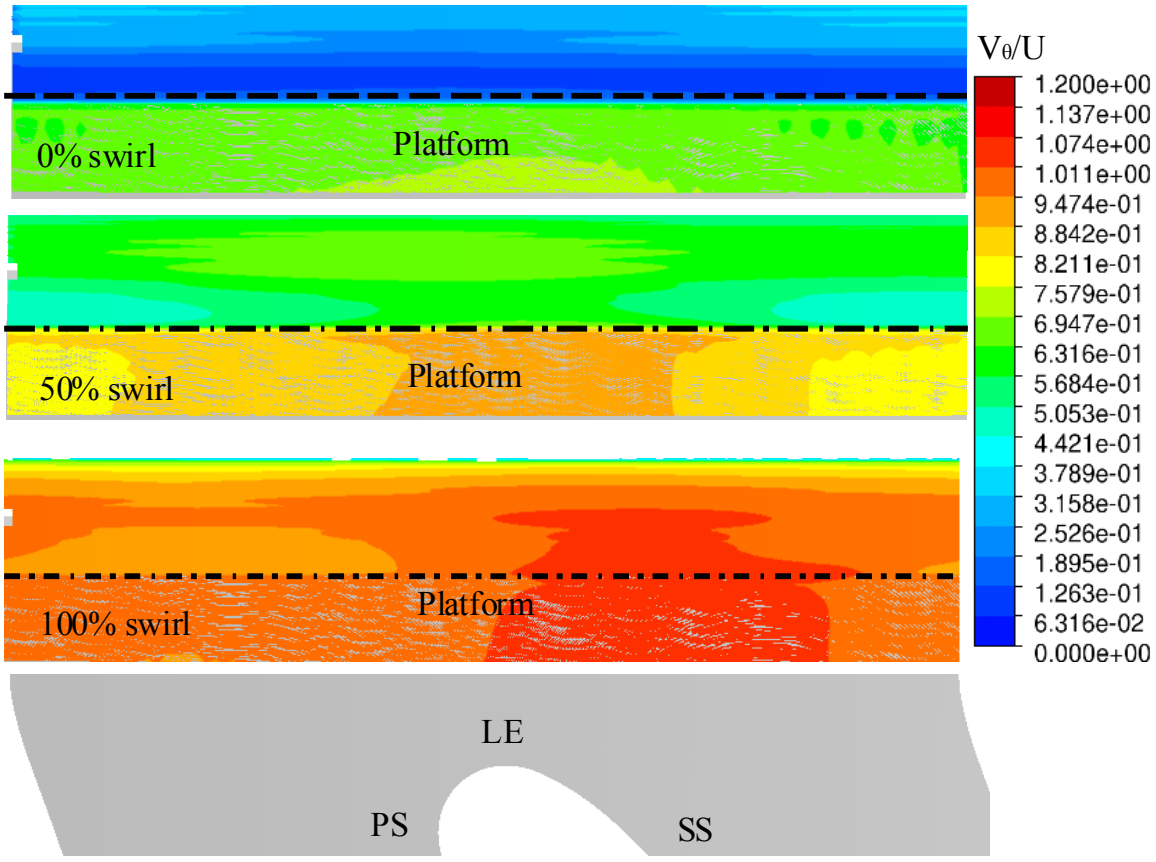


**Figure 23: Baseline- Swirl at the Interface**

When looking at the swirl locally for Contour #1 (Figure 24), the contours show that at 0% swirl the circumferential contour has the least swirl at the tip, but higher swirls at the area where the contour begins to become straight. For 50% swirl the flow seems to have more swirl at the tip, when compared to the Baseline (Figure 23). For 100% swirl, the higher swirls are found at the same location as the Baseline, that is, at the suction side of the blade, with values of almost 115% swirl, while the swirl gets sacrificed at the pressure side. Thus, as mentioned previously, the secondary flow structure will be changed by the contours regardless.

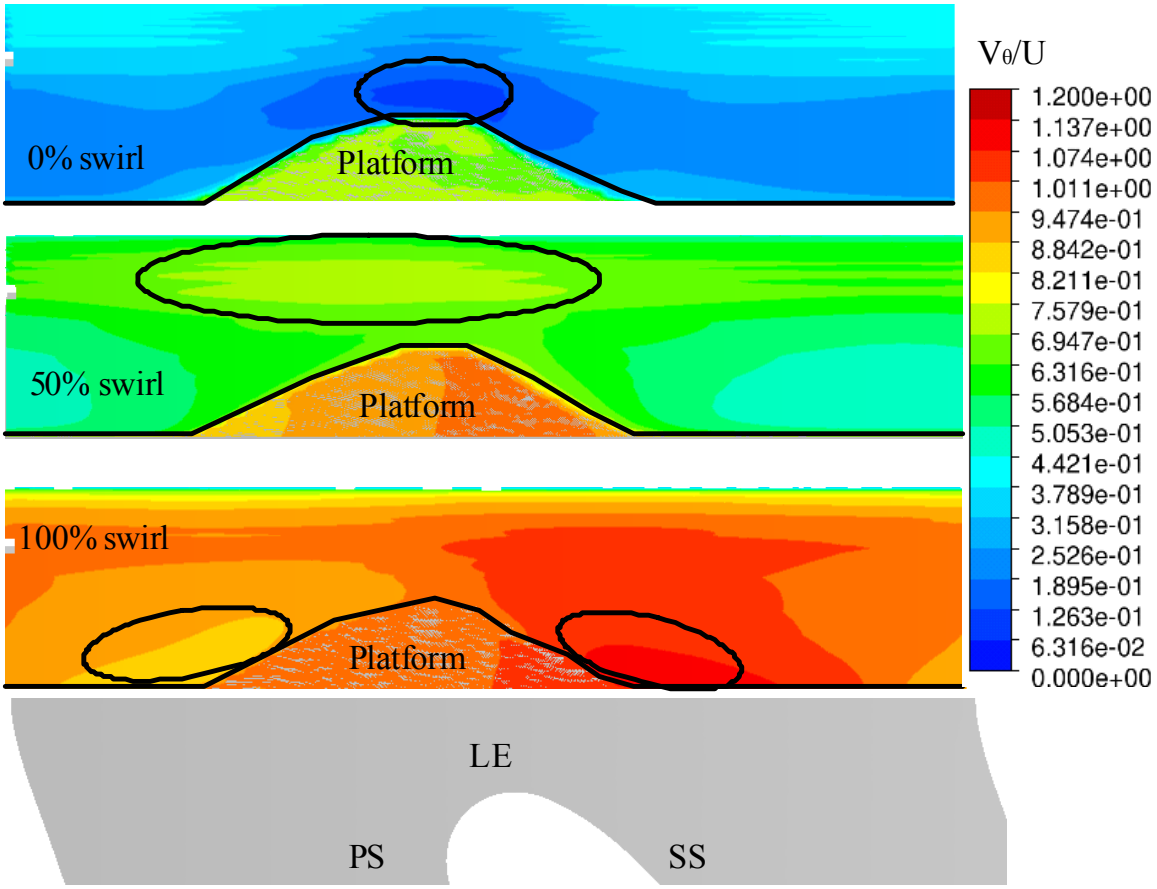


**Figure 24: Contour 1: Swirl at the Interface**

Figure 25 contains the swirl at the interface for Contour #2. A general trend found by comparing Contour# 1 to Contour #2 at 0% swirl shows that the lowest tangential velocities are located at the pinnacles of contours, while higher swirls are manifest at the straighter areas of the platform. At higher swirls, Contour #2 is highly manipulating the behavior of the flow, because it is located where the flow would naturally have the least swirl. This might be allowing for the flow to pick up some swirl but at the locations were the impact will not be beneficial for reducing loss. For Contour #2 at 100% swirl, it can be seen that the swirl is affected by the static pressure distribution due to the contour. Higher swirls remain close to the suction side, and lower swirls close to the pressure side. Again, because the swirl is being manipulated by the contour, the flow therefore changes the secondary flow structure, but not at a location where it helps it reduce loss.

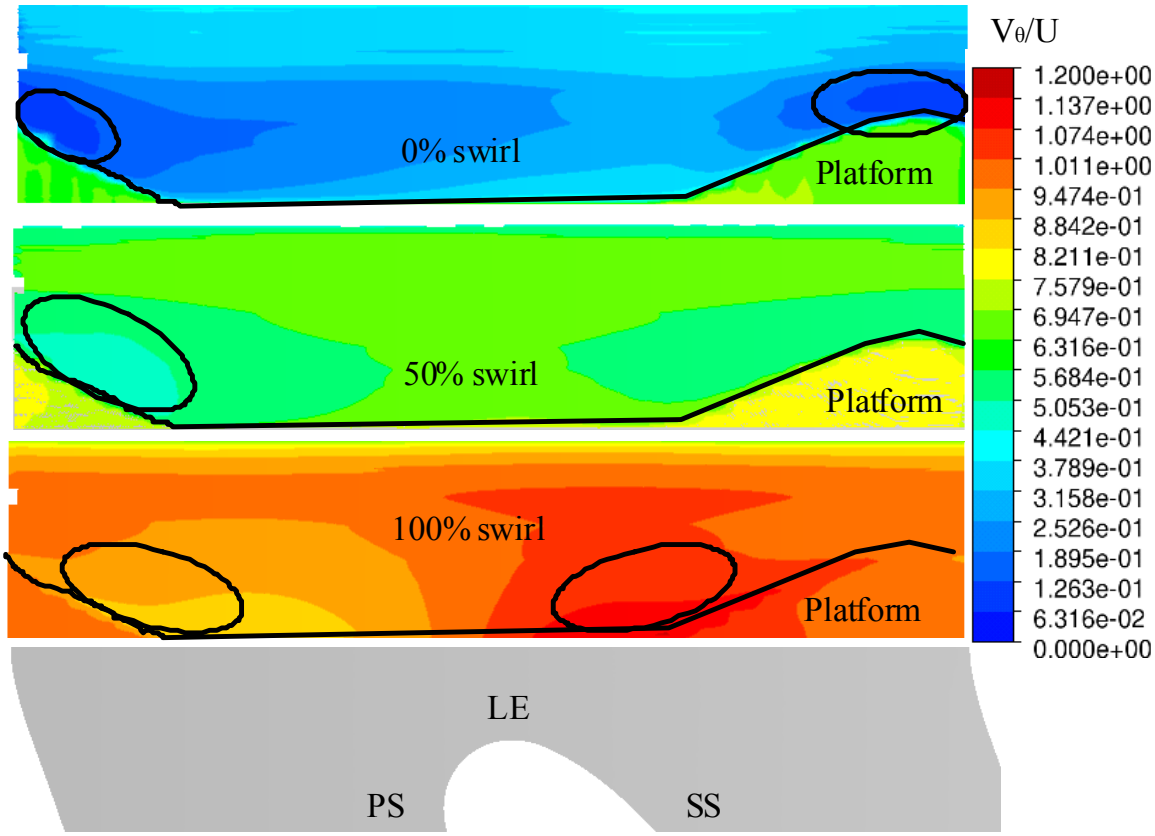


**Figure 25: Contour #2- Swirl at the Interface**

Overall, again, because of the location at where the contour occurs at Contour #1 the secondary flow gets manipulated at the correct location where when the flow exits the cavity it manipulates the secondary flow to the extent that it generates fewer losses.

## 4.5 Entropy Generation

Figure 26 shows the work lost due to viscous effects for Contour #1. Equation 1 (also visible in Figure 26) shows how the work is related to entropy generation. As mentioned earlier, the entropy generated is highest at 0% swirl. It is evident in Figure26 how at 50% swirl there is less loss generated. Also, when reaching 100% swirl there is the least entropy generated. This is in accordance to all of the results in the literature, more specifically, those presented by Reid et al. (2005) and Demagne and Longley (2000) (mentioned above). A clear trend shows that as the swirl is increased, less loss due to viscous effects is generated. It is also relevant to mention that as the swirl is increased beyond 50% the breach of loss gets smaller, which allows for the author to conclude that increasing swirl beyond 50% will begin to reduce the amount of benefit. Therefore, swirling the flow to 100% might have a high cost and not a great reduction in loss. But swirling to about 75% might have a higher benefit since higher swirls can be obtained locally by applying contours in the circumferential direction.

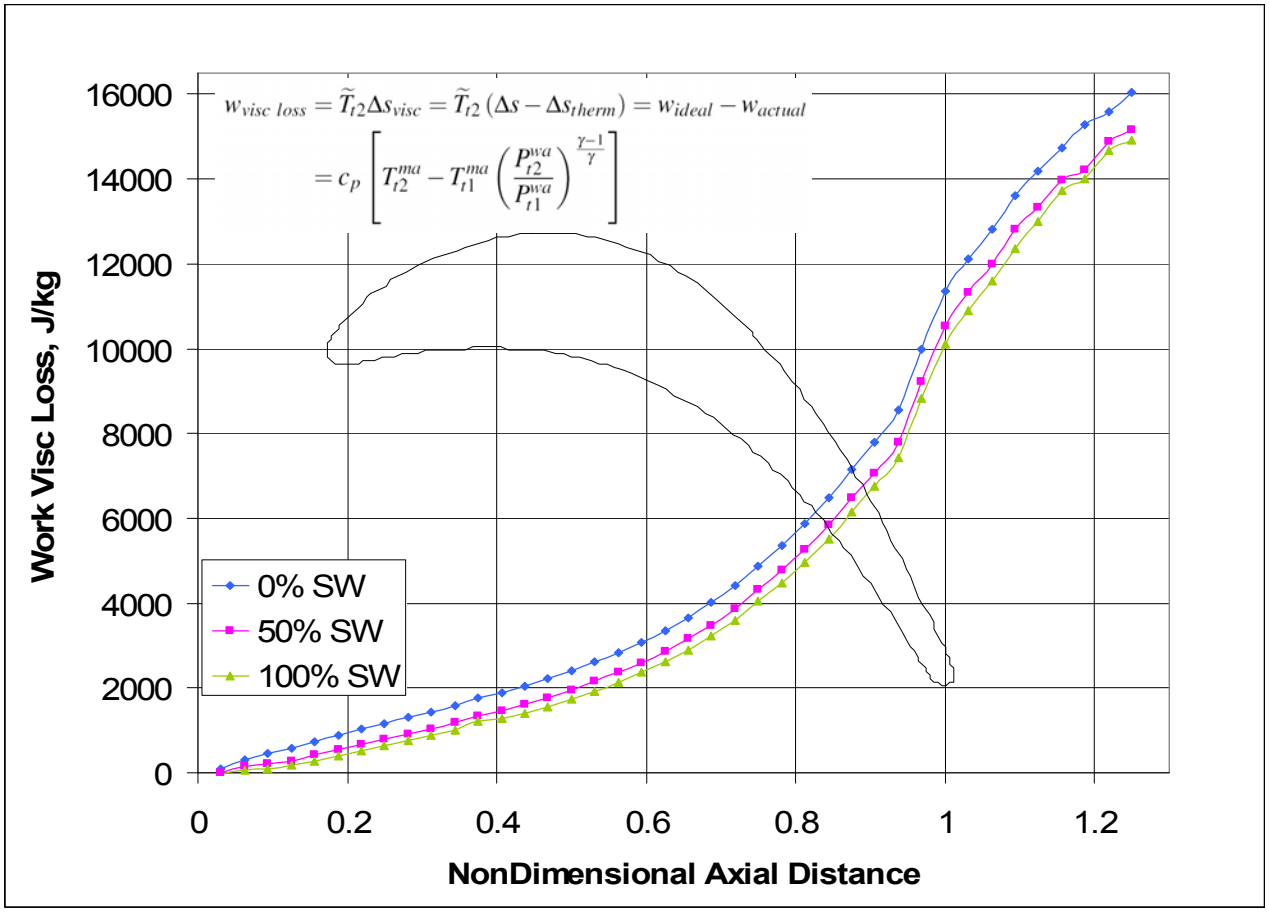


**Figure 26: Work Lost due to Viscous effects for C1 at Different Swirls**

## 4.6 Efficiency

The efficiencies for all of the operating conditions for each platform (Baseline, Contour #1, and Contour #2) were calculated using Equation 2. This equation provides for the mass flow at the cavity to be taken into account. The efficiencies are plotted in Figure 27. Contour #1 has the best performance for 50% swirl, while the baseline has the best performance for 0% and 100% swirl. These results demonstrate that the contours work better at some conditions than others. However, even at 100% swirl both the baseline and Contour #1 perform the same, so it is possible to assume that at higher swirls Contour #1 would perform better than the baseline.

$$\eta_{br} = \frac{T_q \omega}{\dot{m}_m c_p T_{01m}\left(1 - \left(\frac{\overline{P_{03}}}{P_{01m}}\right)^{\frac{\gamma-1}{\gamma}}\right) + \dot{m}_s c_p T_{01s}\left(1 - \left(\frac{\overline{P_{03}}}{P_{01s}}\right)^{\frac{\gamma-1}{\gamma}}\right)} \quad \textbf{(Ref.13)} \qquad \textbf{(2)}$$

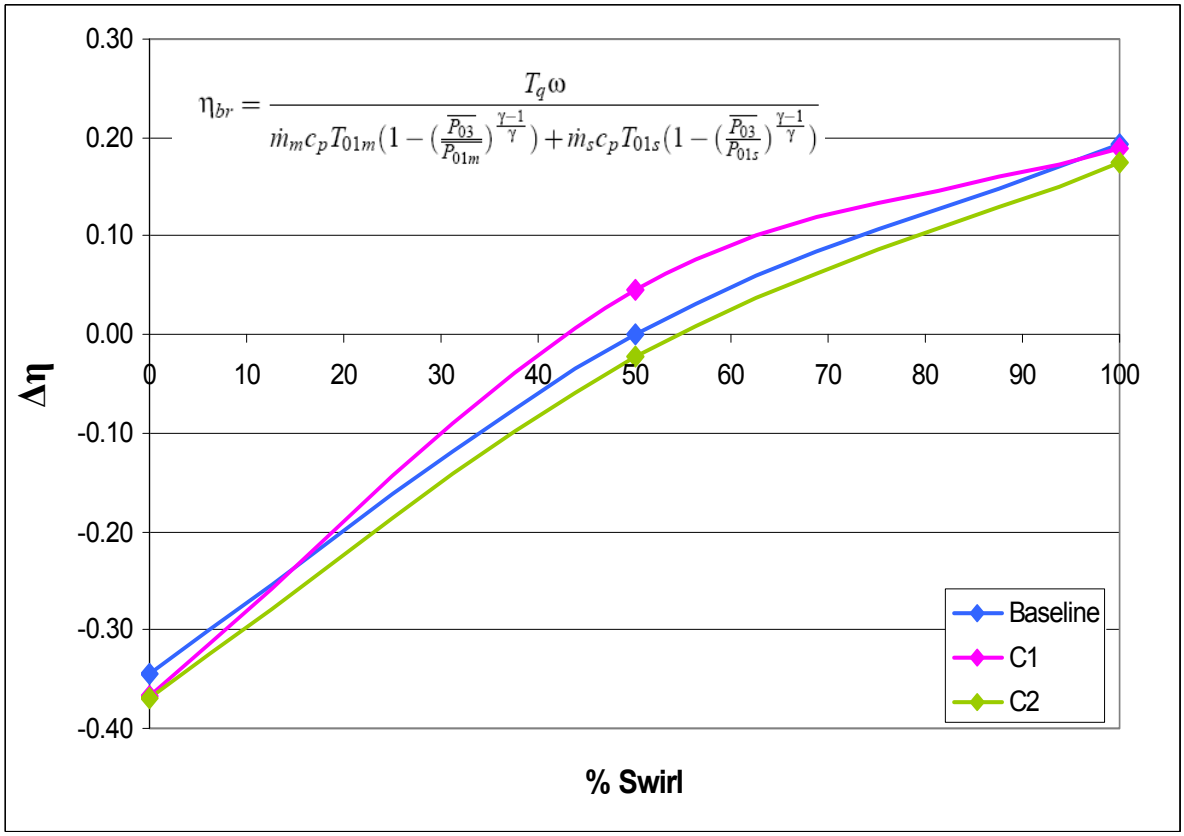


**Figure 27: Efficiency**

## 4.7 Results at Lower Mass Flow Rates

Due to projections for the future in reducing purge mass flow rates, the results for the trends at lower mass flows will be presented in this section. Only one level of swirl was selected: 50% swirl.

The following three figures present the total pressure loss coefficient plots and the vortex intensity for the Baseline, Contour #1, and Contour #2 at the conditions mentioned above. Figure 28 shows how the vortices begin to form at the leading edge. There are two main differences between the models. Contour #2 has an additional vortex moving from the pressure side to the suction side (same as the 1.5% mass flow rate case) and the intensity of the vortices is different for all of the cases. The lowest intensity vortex at the leading edge occurs for Contour # 2 at 57,960. The $C_{PT}$ loss plots do not show a large difference in loss, only that at the curves are different up to about 5%, which shows a small influence from contour to contour. The $C_{PT}$ plot also shows how Contour #2 is generating higher losses than the other contours, however, only by 1-2%.

The Mid-Chord, illustrated in Figure 29, shows how the highest loss generator is Contour #2 as well. The $C_{PT}$ curves show that the contours are having an effect on the flow up to about 18% span. The vortex intensity contours agree with these results as Contour #2 has the vortex with the highest intensity migrating upwardly. As mentioned before, this is not a good condition to reduce loss because when the vortex migrates up the span the blade will be hindered from extracting work from the main flow. The other two models (Baseline and Contour #1) contain vortices that are starting to form at 50% chord and therefore will not migrate upwardly until they are completely formed.

The last plot at a lower mass flow rate (0.5% main flow) is shown in Figure 30. It is remarkable that the $C_{PT}$ curves are different because it means that the contours are affecting the flow even at a significantly lower mass flow rate. At the passage vortex location the least loss is generated by Contour #1, which remains consistent with the trends found at 1.5% mass flow. Additionally, the highest loss generator is still Contour #2. If we look at the plot from 5-20% Contour #1 is generating the highest loss, but because this is at a location that the vortex is not located at, the impact is not large in the overall. The vortex intensity plots show that the vortex with the least strength is contained in Contour #1 and the one with the highest strength is in Contour #1. This is consistent with what was mentioned above. Therefore, Contour #1 at lower mass flow rates is still the location where the design must be applied.

Due to projections for the future in reducing purge mass flow rates, the results for the trends at lower mass flows will be presented in this section. Only one level of swirl was selected: 50% swirl.

The following three figures present the total pressure loss coefficient plots and the vortex intensity for the Baseline, Contour #1, and Contour #2 at the conditions mentioned above. Figure 28 shows how the vortices begin to form at the leading edge. When comparing the total pressure loss with the 50% swirl at 1.5% mass flow rate model, it becomes clear that the vortex is lower in span. Because it is known that reducing the mass flow rate percentage reduces the loss, this discussion will be focused more on the formation of the vortices and how the contours manipulate the secondary flow. There is an impact on loss when reducing the mass flow rate. This occurs because the passage vortex has less strength and height

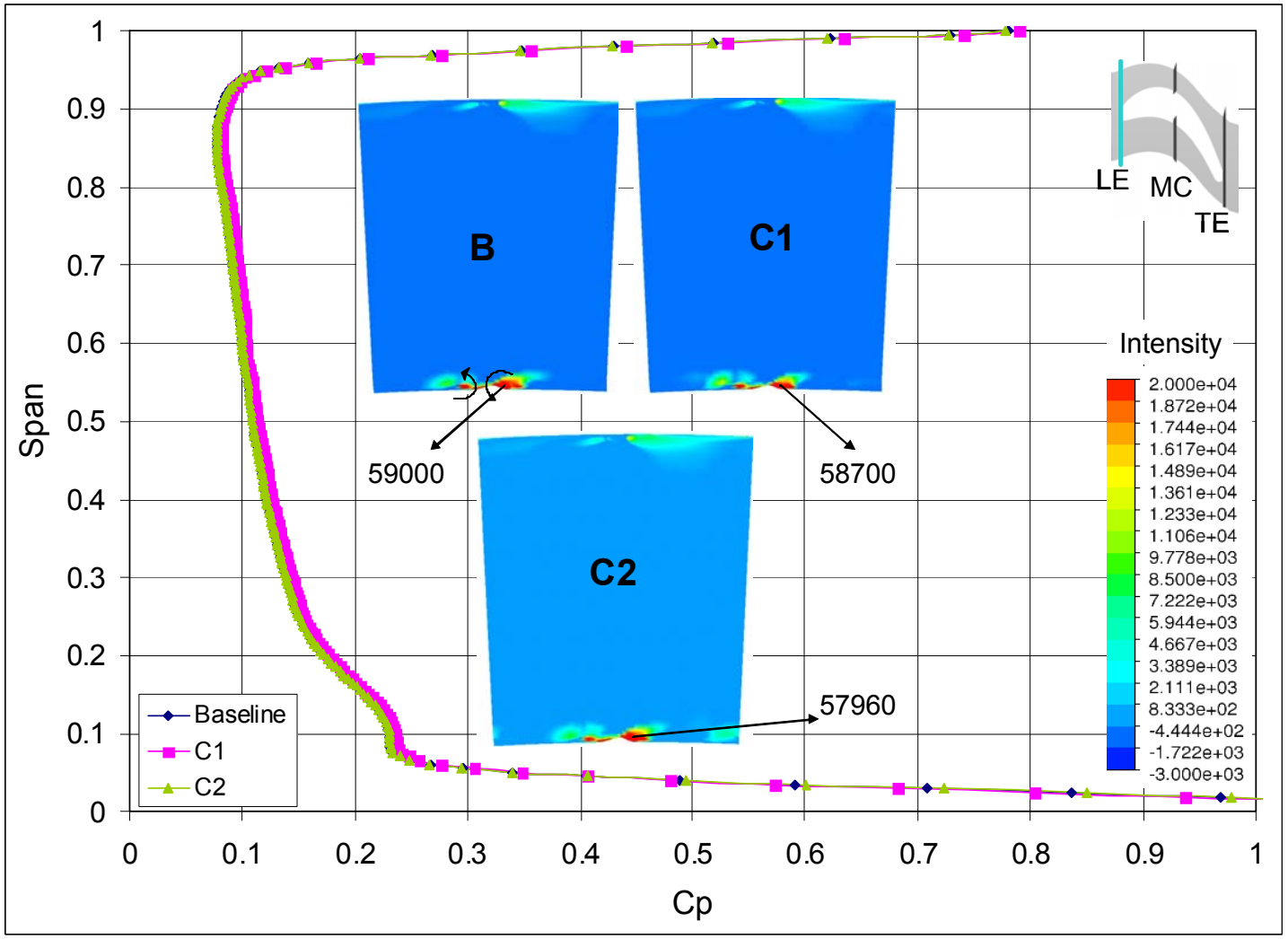


**Figure 28: Leading Edge $C_{PT}$ and Vortex Intensity at 50% swirl for 0.5% Purge Mass Flow Rate**

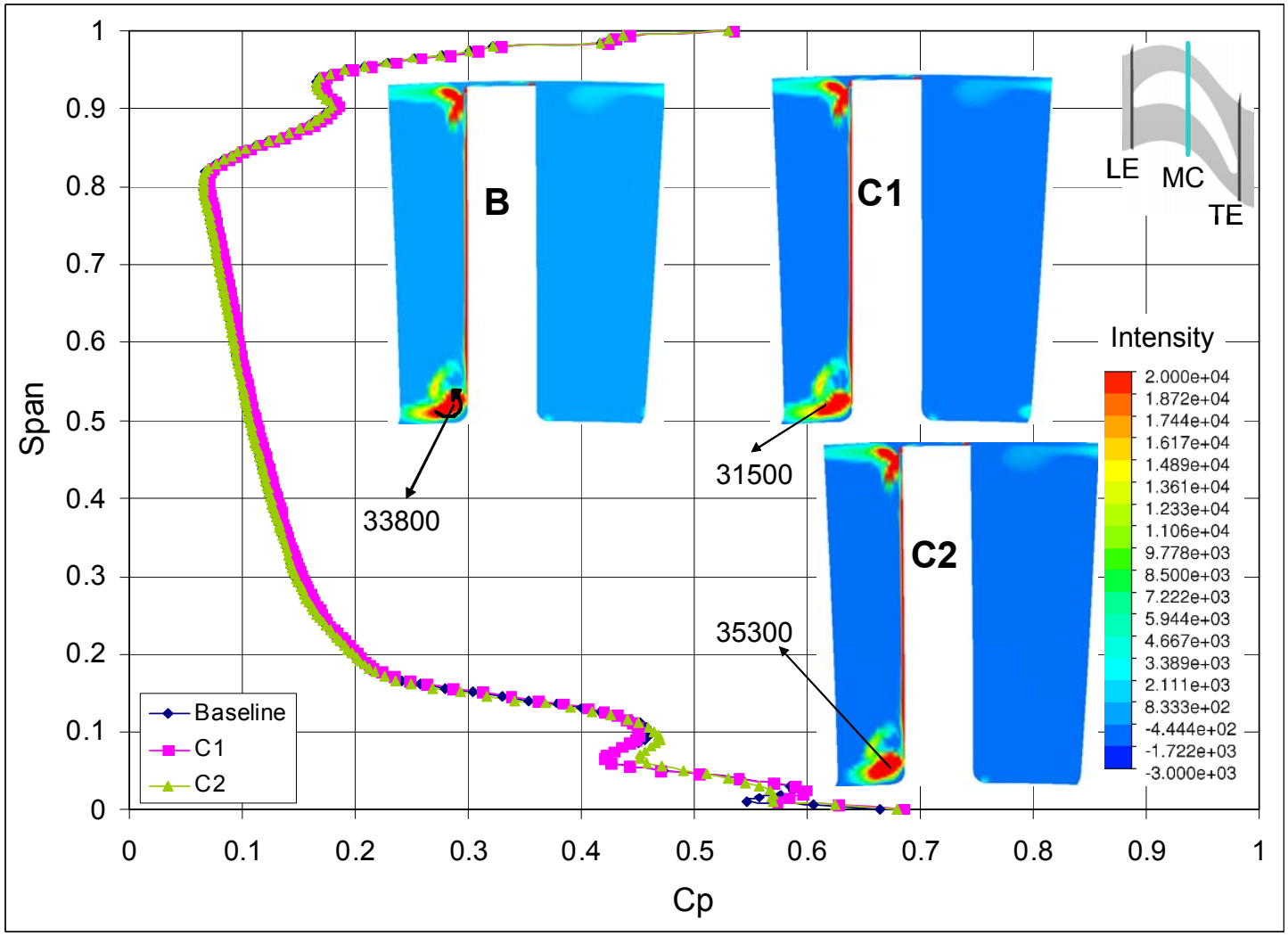


**Figure 29: Mid-Chord $C_{Pt}$ and Vortex Intensity at 50% swirl for 0.5% Purge Mass Flow Rate**

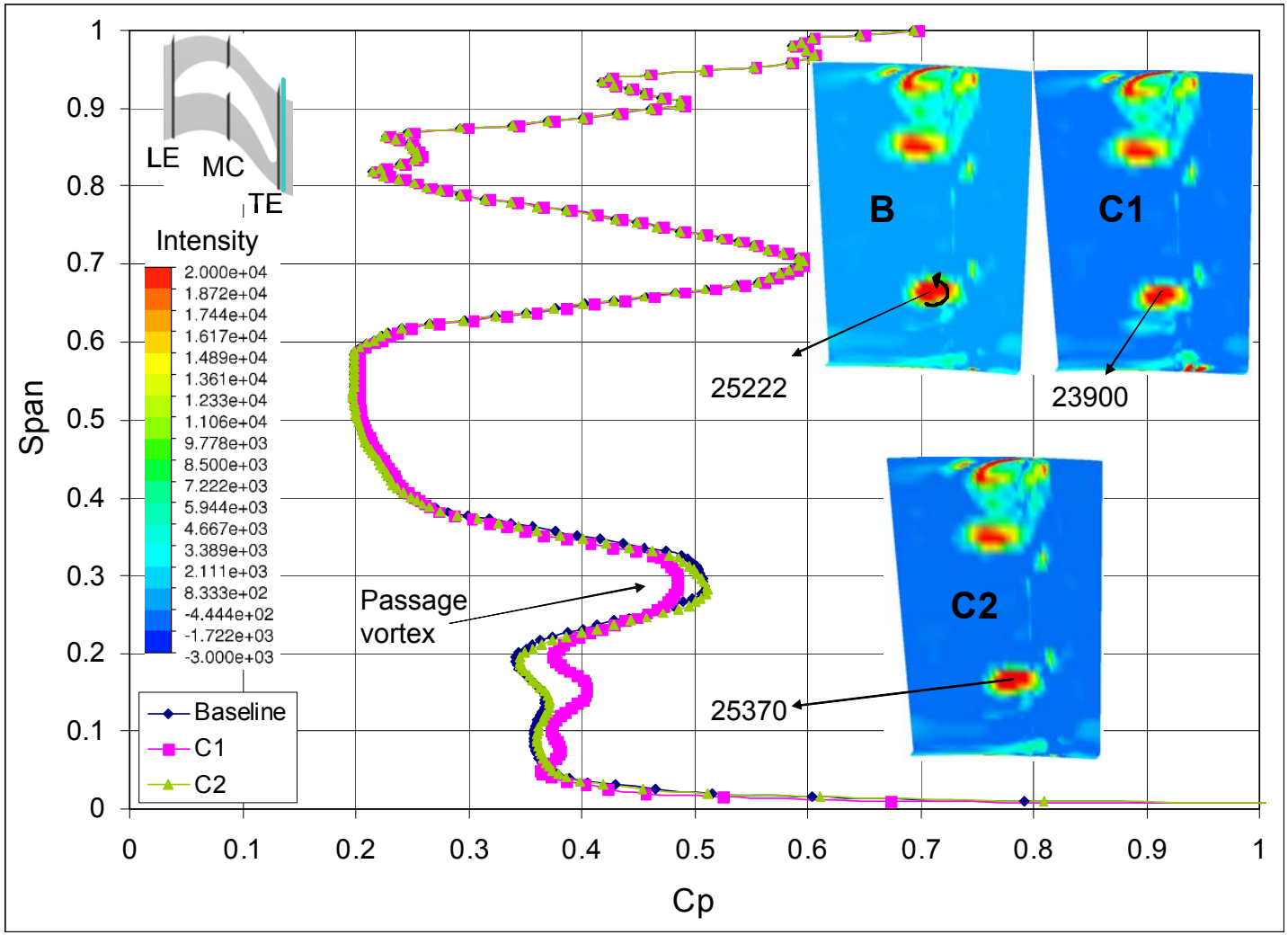


**Figure 30: Trailing Edge $C_{Pt}$ and Vortex Intensity at 50% swirl for 0.5% Purge Mass Flow Rate**

# CHAPTER FIVE:
# CONCLUSIONS AND RECOMMENDATIONS

## 5.1 Conclusions

Effects in the circumferential direction have shown a difference in the secondary flow behavior and losses. The secondary flow was definitely affected at the leading edge region and the effects caused changes far downstream until the wake region. The vortex intensity contours along with the $C_{PT}$ loss plots demonstrated how having a contour aligned with the blade leading edge is beneficial for reducing loss. However, overall efficiency demonstrated that the swirl condition at the cavity plays a big role in circumferential contouring. Swirls in the 50% region are best for contours aligned with the blade leading edge (i.e. C1).

The results for lower mass flow rates show that the contours still have an impact on the flow. Therefore designing at the location of Contour #1 would manipulate the secondary flow to the designer's advantage.

## 5.2 Recommendations

These proposed contours already demonstrate some aerodynamic improvement. However, further refinement of the platform geometry can be done in order to control the secondary flow and generate the least loss. A novel design has already been proposed in the patent by Lee et al. (2011).

Future work lies on understanding how the contours affect the ingestion of hot gasses into the cavity. It would also be beneficial to perform unsteady calculations. This would ensure the results are comparable to a real engine and could be implemented accordingly. Additionally, the contours should be tested experimentally, to validate the results of this study.

# APPENDIX A:
# COPYRIGHT ASSIGNMENT

**SIEMENS**

## COPYRIGHT ASSIGNMENT AGREEMENT FOR PAPER

The undersigned author(s), for good and valuable consideration, hereby grant(s) and assign(s) (for US Government authors, this provision applies only to the extent that copyright is transferable) all rights, title, and interest as protected by US copyright laws (both statutory and common law) in the paper identified below to Siemens Energy, Inc.:

Title of paper or article: **Purge and Mainstream Flow Interaction Control by Means of Platform Circumferential Contouring**

Authors:

| Author | Company | Date | Signature |
|---|---|---|---|
| Melissa Harris | SEI | 07/27/2011 | |
| Jayanta Kapat | UCF | 07/27/2011 | |
| | | | |

By: John Muscne

Author's Employer Company/Entity: SEI / UCF

Date: 7/27/11

Siemens Energy, Inc.

4400 Alafaya Trail
Orlando, FL 32826-2399

2 (Release to SEI-12-2036 (2).doc)

# APPENDIX B:
# ENTROPY AS A MEASURE OF LOSS

**Adapted from Zlatinov et al. (2011)**

Entropy generation due to irreversible processes can be related to lost opportunity to do work in a turbine.. It will also be shown that volumetric entropy generation rate can be a useful tool for tracing losses to responsible flow features. For these reasons the authors have chosen to use entropy generation as the measure of loss. However, it is important to realize that entropy generation due to thermal mixing is not a loss with respect to the turbine but rather to the cycle, and in assessing turbine performance one must consider viscous effects only. This section presents a method for isolating viscous losses in the context of multi-stream and non-uniform flow expansion.

Consider first the scenario of multiple streams of working fluid with distinct inlet conditions being expanded through a turbine to the same downstream stagnation pressure. One way of dealing with such an expansion is by tracing each individual fluid stream as it expands through the turbine, but a much more practical approach is illustrated in Fig. B1 for the case of two streams, a and b. The first step is to replace the non-uniform inlet flow with an equivalent uniform flow that would produce the same work output if expanded through a turbine. To obtain an appropriate average stagnation pressure, consider the thought experiment in which the higher pressure stream is expanded isentropically to a pressure $P^{wa}_{t1}$ such that the work output from this process is just enough to compress the lower pressure stream to the same $P^{wa}_{t1}$ . This process generates no net work, and essentially describes the useful concept of "work-averaging". Work-averaged pressure is applicable not only for dealing with multiple discrete streams but also with continuous non-uniformities in stagnation pressure. The expression for work-averaged pressure is reproduced here in Eqn. (B1) Returning to the simple example of two discrete streams, mass flow averaging of stagnation temperature allows us to fix the state of the substitute uniform flow,

while enforcing energy conservation. Expanding this hypothetical uniform flow, with inlet conditions $P^{wa}_{t1}$ and $T^{ma}_{t1}$ , to any downstream pressure will yield the same work output as if the two original streams were expanded independently to that same downstream pressure. The "ideal" work output of these two streams is therefore readily given by Eqn. (B2).

However, the qualifier "ideal" has been put in quotations because mass flow averaging of stagnation temperature amounts to thermal mixing at constant pressure. This process is irreversible and generates an amount of entropy $\Delta s_{therm}$, as indicated in Fig. B1. Theoretically, a heat engine could have been used to bring the two streams into thermal equilibrium reversibly, generating additional work amounting to $eT_{t2}\Delta s_{therm}$. In practice, this cannot be accomplished with a simple turbine, and the thermal mixing loss is unavoidable. Therefore, as far as a turbine component is concerned, $w_{ideal}$ alone is the relevant ideal work. The irreversible thermal mixing that generates $\Delta s_{therm}$ is not a debit to turbine performance but rather a cycle loss that will be accounted for most rigorously through cycle analysis. In an expansion process through a non-ideal turbine entropy will also be generated due to viscous effects, $\Delta s_{visc}$, with attendant lost opportunity to do work given by Eqn. (B3). It is only these viscous losses that are of interest to the turbine designer, and it is crucial that entropy generated by viscous effects is isolated from total entropy generated. For steady flows, Eqn. (B3) provides a convenient way of doing this with work-averaged stagnation pressure and mass-averaged stagnation temperature.

$$P_t^{wa} = \left[ \frac{\int T_t \, dm}{\int T_t / P_t^{\frac{\gamma-1}{\gamma}} \, dm} \right]^{\frac{\gamma}{\gamma-1}} \qquad \textbf{(B1)}$$

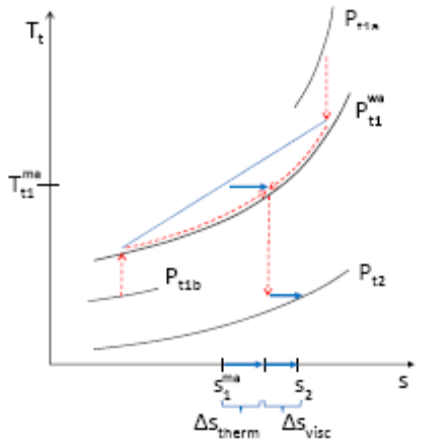


**Figure B1: T-S Diagram of Multi-Stream Expansion**

$$w_{ideal} = c_p T_{t1}^{ma}\left[1-\left(\frac{P_{t2}^{wa}}{P_{t1}^{wa}}\right)^{\frac{\gamma-1}{\gamma}}\right] \tag{B2}$$

$$\begin{aligned} w_{visc\ loss} &= \tilde{T}_{t2}\Delta s_{visc} = \tilde{T}_{t2}\left(\Delta s - \Delta s_{therm}\right) = w_{ideal} - w_{actual} \\ &= c_p\left[T_{t2}^{ma} - T_{t1}^{ma}\left(\frac{P_{t2}^{wa}}{P_{t1}^{wa}}\right)^{\frac{\gamma-1}{\gamma}}\right] \end{aligned} \tag{B3}$$

# APPENDIX C:
# PATENT DRAWINGS RELATED TO THIS WORK

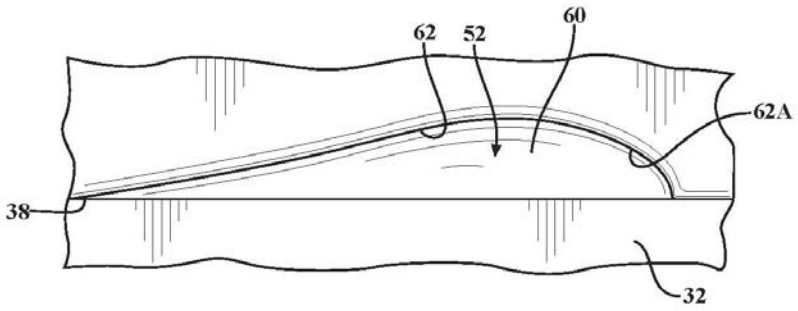


FIG. 3A

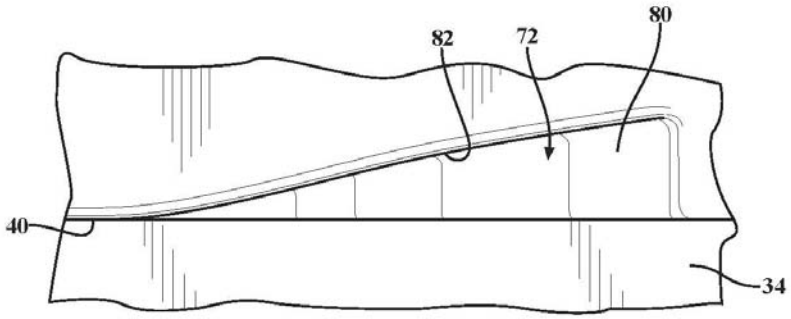


FIG. 5A

Patent application[8]: 2010P26642US

# LIST OF REFERENCES


Akturk, A. & Camici, C. (2011). Tip Clearance Investigation of a Ducted Fan Used in VTOL UAV's, Part 2: Novel Treatments via Computational Design and their Experimental Verification. *ASME Turbo Expo Proceedings* (GT2011-466359).

Benner, M. W., Sjolander, S. A., & Moustapha, S. H. (1997). Measurements of Secondary Flows in a Turbine Cascade at Off-Design Incidence. *ASME Turbo Expo Proceedings* (97-GT-382).

Chakraborty, P., Balachandar, S., & Adrian, R. J. (2005). On the Relationships between Local Vortex Identification Schemes. *Journal of Fluid Mechanics*, *535*, 189-214.

Chong, M. S., Perry, A. E., & Cantwell, B. J. (1990). A General Classification of Three Dimensional Flow Fields. *Physics of Fluids A, 2* (5), 765–777.

Christensen, K. T. & Adrian, R. J. (2002). The Velocity and Acceleration Signatures of Small-Scale Vortices in Turbulent Channel Flow. *Journal of Turbulence*, *3*, 1-28.

Demagne, A. A. J. & Longley, J. P. (2000). The Aerodynamic Interaction of Stator Shroud Leakage and Mainstream Flows in Compressors. *ASME Turbo Expo Proceedings* (GT2000-570).

Denton, J. D. (1993). Loss Mechanisms in Turbomachines. *ASME Journal of Turbomachinery*, *115*, 621-650.

Girgis, S., Vlasic, E., Lavoie, J. P., & Moustapha, S. (2002). The Effect of Secondary Air Injection on the Performance of a Transonic Turbine Stage. *ASME Turbo Expo Proceedings* (GT2002-30340).

Harvey, N. W., Rose, M. G., Taylor, M. D., Shahpar, S., Hartland, J. C., & Gregory-Smith, D. G. (2000). Non-Axisymmetric Turbine End Wall Design: Part I- Three-Dimensional Linear Design System. *ASME Journal of Turbomachinery*, *122* (2), 279-285.

Langston, L. S. (2001). Secondary Flows in Axial Turbines- A Review. *Annals of New York Academy of Sciences*, *934* (1), 11-26.

Lee, C.P., Tham, K. M., Harris, M., Vitt, P., Williamson, S., Prakash, C., & Montgomery, M., Siemens Energy, Inc., Orlando FL, U.S. Patent Application for "Flow Directing Member for Gas Turbine Engine", 2010P26642US, filed July 12, 2011.

Reid, K., Denton, J. Pullan, G. Curtis, E., & Longley, J. (2005). The Interaction of Turbine Inter-Platform Leakage Flow with the Mainstream Flow. *ASME Turbo Expo Proceedings* (GT2005-681551).

Reid, K., Denton, J., Pullan, G., Curtis, E., & Longley, J., (2006). The Effect of Stator-Rotor Hub Sealing Flow on the Mainstream Aerodynamics of a Turbine. *ASME Turbo Expo Proceedings* (GT2006-90838).

Rose, M.G. (1994). Non-Axisymetric Endwall Profiling in the HP NGV's of an Axial Flow Gas Turbine. *ASME Turbo Expo Proceedings* (GT1994-249).

Schupback, P., Rose, M.G., & Gier, J. (2009). Influence of Rim Seal Purge Flow on Performance of an Endwall-Profiled Axial Turbine. *ASME Turbo Expo Proceedings* (GT2009-59653).

Sieverding , C. H. (1985). Recent Progress in the Understanding of Basic Aspects of Secondary Flows in a Turbine Blade Cascade. *ASME Journal of Engineering Gas Turbines and Power*, *107* (2).

Wang, H. P., Olson, S. J., Goldstein, & R. J., Eckert, E. R. G. (1997). Flow Visualization in a Linear Turbine Cascade of High Performance Turbine Blades. *Journal of Turbomachinery*, *119*, 1-8.

Zhou, J., Adrian, R. J., Balachandar, S., & Kendall, T. M. (1999). Mechanisms for Generating Coherent Packets of Hairpin Vortices in Channel Flow. *Journal Fluid Mechanics*, *387*, 353–396.

Zlatinov, M., Tan, C.S., Montgomery, M., Islam, T., & Seco-Soley, M. (2011). Turbine Hub and Shroud Sealing Flow Loss Mechanisms. *ASME Turbo Expo Proceedings* (GT2011-46718).